Joint Centre for Mesoscale Meteorology, Reading, UK

A Polar Low Outbreak: Evolution and Mesoscale Structures

T. D. Hewson
G. C. Craig
C. Claud

Internal Report No. 45

February 1995

Met Office Joint Centre for Mesoscale Meteorology Department of Meteorology
University of Reading PO Box 243 Reading RG6 6BB United Kingdom
Tel: +44 (0)118 931 8425 Fax: +44 (0)118 931 8791
www.metoffice.com

Designed and produced by the Met Office © Crown copyright 2001 01/0240 The Met Office logo is a registered trademark.

A Polar Low Outbreak: Evolution and Mesoscale Structures.

T. D. Hewson, G. C. Craig
and C. Claud[1].

Abstract:

Detailed mesoscale analyses have been performed of a train of four polar lows which developed over the north Atlantic, in March 1992, on the southwestern flank of an outbreak of exceptionally cold arctic air. Operational forecasts from numerical models during this period were uncharacteristically poor. Although the polar lows were considerably smaller than standard mid-latitude depressions a number of structural and evolutionary similarities were identified, notably (mesoscale) warm and cold fronts, a cloud head and frontal fracture. These similarities became more prevalent when the low level baroclinicity was enhanced.

We describe, in detail, the evolution of each low. We also provide for forecasters new guidance pertaining to polar low outbreaks, covering recognition and analysis of lows and (mesoscale) fronts, precipitation distribution and intensity, and interpretation of satellite and radar imagery. For the final, most intense low, which generated winds in excess of 70 knots, we describe and attempt to explain aspects of its three-dimensional structure around the time of maximum intensity. One notable feature was a large area of persistent heavy snow to the left of its track, beneath a cloud head. This was caused by slantwise ascent in a region of slantwise convective instability, and not by upright convection. This was in spite of the air being rendered exceptionally unstable to upright convection by the temperature of the underlying sea surface.

1: Introduction

Relative to standard mid-latitude cyclones polar lows generally have small horizontal and vertical length scales, and short lifetimes. They also tend to occur in data-sparse regions. For these reasons predicting and verifying their evolution is problematic. Knowledge of this behaviour is however important, for polar lows frequently give rise to hazardous weather, notably severe winds and heavy snowfall, and may also contribute significantly to the global energy budget, on account of the large sea surface fluxes of heat and moisture frequently associated with them.

This study will describe, in detail, four polar lows which developed in the north Atlantic during a three day period in March 1992. We subsequently refer to this period (12th/00UTC to 15th/06UTC) as the 'polar low outbreak'. During this outbreak the main short-range forecasting model of the U.K. Meteorological office produced inaccurate analyses and misleading forecasts (compare 24-hour model forecasts in Fig. 10b with our corresponding analyses in Fig. 10a) and hence gave an initial motivation for the work. The Norwegian operational numerical model also performed badly during this period (see figures in Gronas and Kvamsto (1994)). For modellers this study thus provides a dataset and descriptions against which retrospective numerical predictions can be verified. Whilst numerical models continue to have difficulty predicting polar low activity the bench forecaster has to intervene, and thus a second, equally important objective of the work was to provide guidance for forecasters. Specifically this guidance covers recognition and analysis of polar lows, the wind, cloud and precipitation patterns which can be associated with them, and the way in which these features can evolve. With regard to precipitation, we recognise that interpretation of radar data during snowfall presents the forecaster with particular problems, and consider carefully how these may be overcome.

Figure 1 shows that the 'mean track' of the four polar lows ran through a relatively dense network of surface synoptic stations, most (60%) of which reported every hour. In addition many of these stations were on islands whose size, typically a few kilometres across, was probably not large enough to influence the evolution of the lows themselves. This provided an excellent opportunity to study polar lows over the ocean, where they frequently develop and reach maturity. It should also be emphasised that in many past studies surface data coverage has either been far less comprehensive than that shown in Fig. 1, or concentrated on large land masses, where polar lows frequently decay.

Other data sources were also used extensively, notably a ground-based radar (see Fig. 1) and satellite imagery, including specially derived products from the Special Sensor Microwave/Imager (SSM/I) and the TIROS-N Operational Vertical Sounder (TOVS). A key feature of the analysis was the marrying together of data from the different sources, and in the course of this report we make several suggestions of new ways in which this can be usefully performed.

[1] Corresponding author address: Laboratoire de Meteorologie Dynamique du C.N.R.S, Ecole Polytechnique, F - 91128 Palaiseau Cedex. France.

A number of detailed studies of polar lows have been performed in the last few decades, notably Harrold and Browning (1969), Rasmussen (1985) and Shapiro et al (1987). Many such studies concentrate on providing a 'snapshot' in the overall evolution of one particular polar low. For the final, most developmental polar low we also provide a snapshot description of its salient features around the time of maximum intensity, attempting to explain their origins, and making comparison with the aforementioned papers. However an additional aim of our study was to investigate polar lows' *full* evolution, from development through to decay, and we try to do this for each case (Rasmussen (1985) also studied development, though with much less data).

In analysing the polar lows one key result was that we were able to identify, and track, distinct front-like features. Other authors have alluded to the existence of fronts around polar lows, but none, to our knowledge, have been able to track their evolution. Locatelli et al (1982) did investigate frontal evolution, but their cases involved interaction with the main polar front, via an instant occlusion process, and as such are distinct from our cases in which no such interaction occurred.

Investigations of the polar low outbreak and its causes are ongoing. This report represents a first (descriptive) step towards the long term goal of achieving accurate forecasts during such outbreaks.

Section 2 describes the data used, whilst section 3 details the methods of analysis of the lows and their fronts. Section 4 provides an overview of the environment within which the four polar lows developed. Section 5 details the evolution and mesoscale characteristics of each of the lows in turn, whilst section 6 provides the snapshot of the most active low. Our findings are summarised in section 7.

2: Data sources

a) Land-based synoptic observations

Observations from surface synoptic stations shown on Fig. 1 were augmented, at 6-hourly intervals, by radiosonde and pilot balloon ascents from the four stations denoted by squares, and others beyond.

b) Other synoptic observations

At the main synoptic hours (00, 03, .. 21UTC) we also utilised observations from ships. Within the domain of Fig. 1 there were typically 5 of these. Such observations were scrutinised closely, and when necessary corrections made. In particular, pressures were checked for self-consistency with reported pressure tendencies, and general consistency with surrounding data. Pressure reports were also corrected or omitted if the ship call sign appeared on a 'suspect' list. This list is used operationally in the Central Forecasting Office (CFO) of the U.K. Met. Office in Bracknell. It includes ships whose pressure reports over a period of time had consistently differed from the surface pressure predicted by a recent forecast from an operational model. Further checks were made on consistency of ship movements between observations, in order to validate reported position. We found that incorrectly reported positions would have significantly affected the manual surface analysis on several occasions had they not been rectified.

We also utilised observations from North Sea oil rigs, situated principally between the right hand edge of Fig. 1 and the coast of continental Europe. Most reported every three hours but some every hour.

c) Satellite imagery

Many studies of polar lows rely heavily on imagery from polar orbiting satellites (giving a temporal resolution no better than about six hours). This is because polar lows regularly occur at high latitudes for which imagery from geostationary satellites, such as Meteosat, is either not available or severely distorted. The lows studied here occurred sufficiently far south for images from both types of satellite to be used.

i) Geostationary

Hourly Meteosat infra-red images, calibrated to provide cloud top temperature (CTT), were available for the whole period, exceptions being the times 00 and 01UTC when eclipsing rendered the Meteosat imager inoperable. Images were reprojected into a polar stereographic format to reduce high latitude distortion and facilitate direct comparison and overlaying with other data. Parallax errors in the reprojected positions of significant cloud features were considered negligible, on account of the relatively low altitudes of the tops of these features (see Hewson, 1993a). For 14th March 1992

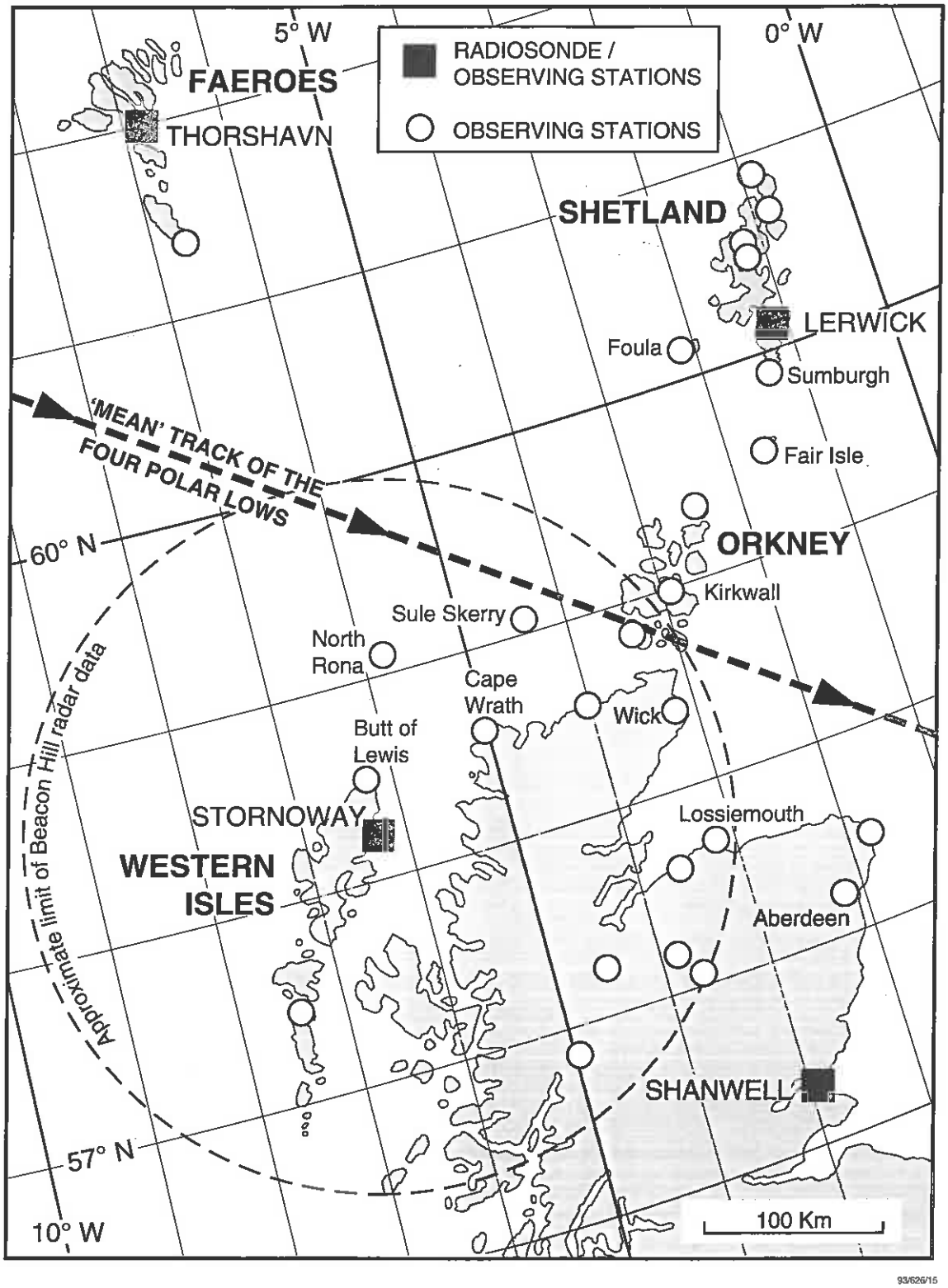

Fig 1: Map of northern Scotland and the Faeroes, representing the main observational region used in this study. Land-based synoptic stations, the approximate area of radar coverage, and the 'mean' polar low track are marked.

selected images from the water vapour channel were also utilised. The high temporal resolution in the imagery enabled the cloud features associated with each low to be successfully tracked.

ii) Polar-orbiting

Polar orbiting satellites have shown their utility for studying polar lows (e.g. Carleton *et al* (1993), Claud *et al* (1993), Turner *et al* (1993)). In addition to standard infra-red and visible imagery, data from the Special Sensor Microwave/Imager (SSM/I) and the TIROS-N Operational Vertical Sounder (TOVS) (see Smith *et al* (1979)) have been used extensively in this study. The average temporal resolution, at a given point, of the standard data was approximately 6 hours; whilst for SSM/I and TOVS data it was about 12 hours.

The SSM/I measures radiation from the earth and atmosphere at microwave frequencies, allowing the calculation over sea of integrated cloud liquid water, surface wind speed, and scattering by large ice particles. The latter is converted into a 'scattering index', a variable which gives a semi-quantitative indication of the degree of convection within a given cloud mass, because large ice particles require rapid updraughts, and hence convection, for their formation. The algorithms used in this study consist of linear combinations of SSM/I brightness temperatures and are described in Claud *et al* (1993).

Soundings from TOVS provide information on the three-dimensional temperature and moisture structure of the atmosphere. The raw TOVS data are converted into atmospheric parameters using the Improved Initialisation Inversion (3I) scheme described in Chedin and Scott (1985) and Chedin *et al* (1985). This scheme relies on use of the TOVS Initial Guess Retrieval (TIGR) dataset which contains about 1800 atmospheric situations and the associated calculated brightness temperatures for each TOVS channel (Escobar, 1993). All parameters are retrieved at a spatial resolution of 100 x 100km, which is a compromise between the spatial resolution of the two major sounders of TOVS: the High resolution Infrared Radiation Sounder (HIRS-2, 17km nadir) and the Microwave Sounding Unit (MSU, 110km nadir).

d) Radar

Early in 1992 two new radars were introduced into the U.K. radar network, both situated in northern Scotland. Some of the first measurements from the Beacon Hill site in the Western Isles have been utilised in this study (see large dashed circle on Fig. 1). The other site was not operational at the time. Data was available for 13th/06UTC to 15th/00UTC.

Evaluation of precipitation generated by polar lows naturally requires 'ground truth'. The regularity with which sub-zero temperatures co-existed with strong winds during this polar low outbreak rendered standard synoptic measurements of rainfall total and snow depth as rather unrepresentative. For this reason attempts have been made to convert radar data into liquid water and snow depth equivalents. This requires some discussion of the radar data itself, which is given below.

The data presented is essentially for a beam elevation of 0.5 degrees, and a beam width of 1 degree. This implies that at a 100km range reflectivity has been averaged between altitudes of about 0.5 and 2.5km, whilst at 200km (the outer limit) averaging is between about 2.5 and 6km. Radar returns are automatically converted from reflectivity, Z, to precipitation rate, R, at source, using the equation $Z=200R^{1.6}$ (note that throughout this paper the variable R and the terms 'precipitation rate' and 'precipitation totals' always refer to *liquid water equivalents*, ie *melted* snow).

An empirical correction which increases the rainfall rate R at ranges above 75km is also applied at source, to try to compensate for overshooting (ie the radar beam being too high). This correction is a multiplying factor for R, which increases linearly to 2.3 at 200km. If precipitation is completely overshot, there will clearly be no correction. Given that convection during the period studied was at times capped by an inversion at heights as low as 2km, complete overshooting must have been a significant source of error at large ranges.

A second error arises in the Z to R conversion indicated above. The constants used are based on rainfall, whereas dry snow was the main form of precipitation observed. Historically the 'standard' equation used for dry snow has been $Z=2000R^2$ (Batten (1973)). However more recent investigations, such as Matrosov (1992) and Thomason (1994, personal communication), have yielded different and probably more reliable constants. Thomason's analysis gave $Z=303R^{2.02}$. This was for a case with *high* aggregate ice density (0.2-0.25 g/cm^3) compared to the data in Matrosov, and as such is probably more representative of the *convective* precipitation observed here.

Table 1 shows how the above equations convert displayed precipitation rates to precipitation rates assuming dry snow, and can be applied to radar data in section 5. There are clearly large differences between the two conversions given for dry snow. Thomason (T) has been used to derive the totals and rates quoted in section 5.

Equivalent grey shading on Fig. 12	Precipitation rate ($mm\,hr^{-1}$) Assuming:			Rate of Snow accumulation ($cm\,hr^{-1}$) (T)
	Rain	Snow (B)	Snow (T)	
Dark ('L') {	0.125	0.06	0.16	0.2
	1	0.32	0.81	1.0
Light ('1') {	4	1.0	2.4	3.0
Medium ('4') {	8	1.7	4.2	5.3
V. Dark ('8') {	16	2.9	7.3	9.1

Table 1: Conversions for radar data in section 5. (B) and (T) are based on calibration constants provided, respectively, by Batten (1973) and Thomason (1994) (see text).

A fifth column was added to Table 1 to give an approximate 'rate of snow accumulation' at the surface, using the Thomason precipitation rate and a standard water to snow depth conversion of 'x12.5'.

In section 5 there are references to precipitation rate (R), to precipitation totals (which we signify by D_R), and snow depth equivalent of D_R derived using a 'x12.5' conversion (which we signify by D_S).

e) Operational models

Data from operational models has also been utilised in this study. These models were the global and limited area (LAM) versions of the U.K. Met. Office unified model (Cullen, 1991). The quoted data is categorised as either 'analysis' or 'forecast'. By 'analysis' we mean the fields derived for time T+0 as part of ongoing, operational, data analysis and assimilation. By 'forecast' we mean fields generated for times beyond T+0.

LAM data was generated by initially extracting the basic variables Φ, U, V, W, T and relative humidity at approximately 100km horizontal and 100mb vertical resolutions, and then deriving other diagnostic quantities from this dataset. As indicated earlier the representation of fine scale detail was poor (it is beyond the scope of this paper to discuss why); however the large scale pattern seemed to be satisfactory (compare panels on Figs 10a and 10b).

3: Methods of analysis

As a first stage in describing the polar low outbreak we compiled a sequence of comprehensive surface pressure analyses (mainly at 3 hour intervals) utilising all the data listed in section 2. This analysis was a complex procedure, involving considerable overlaying, interpolation and extrapolation, both forwards and backwards in time, of data from the different sources. The intention was to maintain continuity between consecutive charts, yet at the same time recognise the appearance and disappearance of significant features. Here we detail the procedures adopted in identifying the polar lows and their fronts. The charts themselves are referenced in sections 4, 5 and 6.

a) Identification of polar lows

For a polar low to be considered to exist at a given time there had to be a localised maximum in the surface geostrophic relative vorticity (ζ_g), as inferred from surface pressure analyses (see appendix I). These vorticity maxima frequently occurred along pre-existing trough-lines; in such cases it was not strictly necessary for there to be an accompanying minimum in the pressure field, although usually there was. Values of ζ_g at individual low centres (quoted in section 5) are generally larger than the surface relative vorticity, ζ, because friction and (particularly) curvature acted to reduce surface wind strength. Although ζ is perhaps more meaningful dynamically, it has to be derived from surface winds which are more difficult to analyse.

b) Identification of mesoscale fronts

For completeness we first define the *general* term 'front'. Here a front is taken to be a boundary at the surface between different airmasses, recognisable as both a discontinuity in temperature and a maximum in relative vorticity.

In the course of preparing surface analyses for this study coherent, small-scale, low-level atmospheric discontinuities were repeatedly identified in connection with the polar lows. These discontinui-

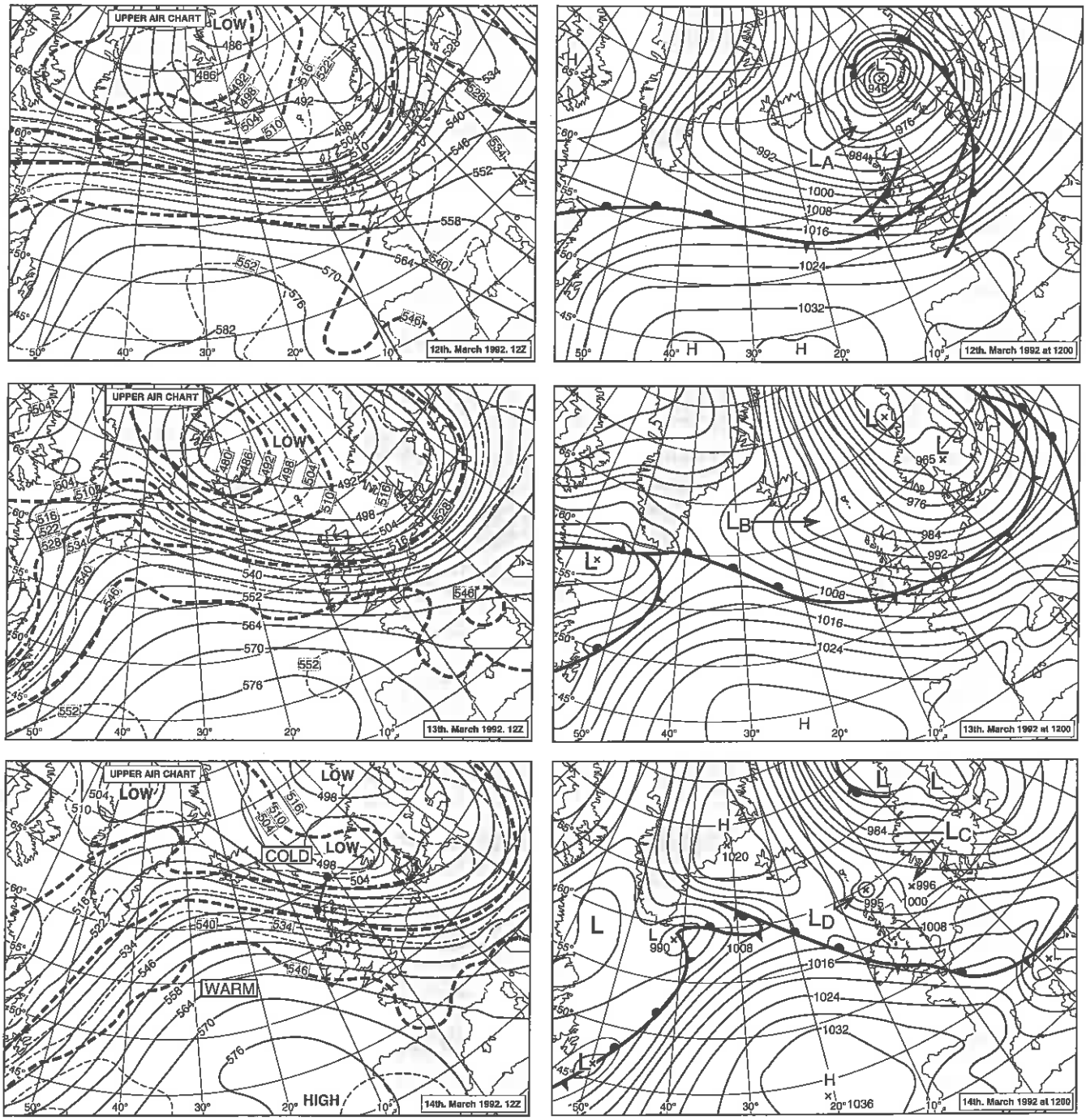

Fig 2: Synoptic charts for 12UTC on 12 (top), 13 (middle) and 14 March 1992 (bottom). **Right** hand panels show *operational* hand-drawn surface analyses (4hPa isobar interval) using conventional classical notation for fronts; labels for polar lows 'A', 'B', 'C' and 'D' have been added. **Left** hand panels show 500hPa height (dam, solid) and 1000-500hPa thickness (dam, dashed) from operational analyses of the global version of the UK Met. Office unified model. The position of the cross-section in Fig. 22 is marked on the lower left panel.

ties could be tracked for many hours. They showed some similarities to classical fronts, but also exhibited important differences - most notably smaller length scales. Because of these differences the discontinuities have been analysed not as *classical* fronts, but as '*meso-*' or '*mesoscale*' fronts (our terminology). The main surface characteristics of these mesoscale fronts are listed below:

(1) a strong vorticity signature,

(2) a lesser (apparent) thermal signature,

(3) narrow bands of mainly convective precipitation (<100 km wide) usually occurring just ahead of the surface trough line,

(4) rapid decay of precipitation on encountering land.

In contrast classical fronts are generally characterised by a strong thermal signature, a weaker vorticity signature, extensive bands of stratiform precipitation falling on the cold air side, and a tendency for this precipitation to propagate large distances across land.

For economy of space we will hereafter be referring to classical fronts as 'classical fronts' and to mesoscale fronts, generally, as just 'fronts'.

It could be argued that the characteristics of mesoscale fronts listed above are similar to those of non-frontal surface troughs. What differentiates (moving) fronts from non-frontal surface troughs is temperature advection. This will show itself, in the case of moving fronts, by there being both a thermal wind with a significant along-front component, and a directional vertical wind shear across any frontal surface. Such features may be more readily identified than a surface temperature discontinuity, for reasons given in appendix II.

In the vicinity of atmospheric discontinuities thought to be mesoscale fronts, we estimated, whenever possible, the thermal wind and geostrophic temperature advection for a layer close to the surface. Because neither pilot nor radiosonde data were generally available in suitable locations these estimates were based on reported surface winds (from just north of mainland Scotland) and velocities of precipitation cells within the frontal zone derived from animated 1/4-hourly radar data. Both velocities were assumed to be geostrophic; and the latter to represent the wind speed at a level in the lower troposphere (taken to be 800hPa). The measurements usually provided evidence of the existence of (mesoscale) fronts, and are quoted in section 5.

4: A Synoptic Overview

The objective of this section is to document the environment, synoptic and otherwise, in which the four polar lows developed. These lows will be referred to as A, B, C and D throughout the study.

Panels on the right of Fig. 2 show CFO operational surface analyses covering the area where the polar lows were identified. The analyses are not definitive; closer scrutiny of all available data reveals considerable structure, as will be detailed later. The analyses do illustrate, however, the broad-scale synoptic environment. They show that polar lows occurred within a broad north to northwesterly airstream on the southwestern flank of a large filling depression. The figures also hint at the existence of a quasi-permanent surface trough oriented west-northwest to east-southeast in the genesis region southeast of Iceland. Such a surface trough has been noted before, in a similar region, during polar low outbreaks (e.g. Mansfield, 1974).

Throughout the period the polar lows remain 700-1000km distant from the main polar front (seen crossing Ireland), indicating that there was no interaction between the two, unlike the cases in Locatelli *et al* (1982).

The 1000-500hPa thickness patterns on the left of Fig. 2 show that very cold air was present, in depth, throughout the period, particularly on the northeastern flank of the mean polar low track (Fig. 1). Also apparent is an increase, with time, in across-track baroclinicity. Comparison with extreme minimum 1000-500hPa thicknesses for March indicates that record values may have been attained (over Shetland, for example) highlighting the exceptional nature of the cold air outbreak. Lerwick, on Shetland, also recorded its lowest daytime maximum for 23 years on 14th, just -3.3°C.

It can be seen from Figs. 1 and 2 that the mean track runs in approximately the same direction as the broad-scale surface flow, the 500mb geostrophic wind vector, and the 1000-500mb thermal wind, indicating that the polar lows were not of the 'reversed shear' type described by Duncan (1978) and Reed and Duncan (1987).

The propensity for polar lows to form tends to increase as the sea-air temperature difference increases (Businger, 1985). In the area around northern Scotland, which is close to the 'mean track' (Fig. 1), sea temperatures are about 8°C (Fig. 3). Air temperatures on 13th and 14th at Kirkwall, a station nearby, averaged about -1°C, giving a sea-air temperature difference of 9°C. This value is

considerably higher than the 5°C mean found by Forbes and Lottes (1985) for 133 polar vortices occurring in a similar region, suggesting that polar low formation could have perhaps been anticipated a priori.

The NOAA visible image in Fig. 4, for 1312 UTC on 12th, shows spirals of convective cloud associated with polar low A, centred near to 60°N 6°W. During the previous 12 hours this low had translated southeastwards from the southeast coast of Iceland, leaving in its wake a cloud band, about 60km wide, also visible on Fig. 4. The line of symbols representing high values of ice scattering index seen west of Low A on Fig. 5, for 1003UTC on 12th, coincided with the cloud band at this earlier time, showing it to be convective in nature. The symbols also lie just on the strong wind side of a near-straight discontinuity in the wind speed field (coloured). Such discontinuities generally occur along trough lines (appendix III), indicating that the cloud band on Fig. 4 was in fact linked to the semi-permanent trough first noted on Fig. 2, on which polar lows B, C and D all subsequently formed. Indeed animated Meteosat imagery showed the cloud band to be just as persistent a feature as the trough line: by 03UTC on 13th the band extended all the way to Denmark; around 13th/06UTC it first broke up, but then reformed southeast of Iceland 3 to 6 hours later.

On Fig. 4 and the re-analysed surface chart in Fig. 6 the trough line was marked as (mesoscale) cold front (C_A) for the following reasons:

(i) ship observations on 12th, although limited, indicated there to be a significant temperature gradient in this region, oriented from south to north. The across-front component of this gradient was about 3°C over 300km (*along* the front $\delta T/\delta P$ was negative).

(ii) observation sequences from Butt of Lewis, North Rona, Sule Skerry, Kirkwall and Fair Isle (Fig. 1) showed there to be a tongue of slightly warmer air just ahead of the front (of width about 150km). Kirkwall, for example, registered a positive temperature perturbation of about 2°C.

(iii) thermal winds and thicknesses for the 1000-850 hPa layer from soundings at 12UTC on 12th were consistent with the existence of a warm tongue.

On figures for later times (principally Fig. 10a) the trough line is denoted as either cold front C_B, cold front Cc or warm front W_D. Nomenclature was selected according to whether advection by the cross-front component of the surface geostrophic wind was cold or warm (as with conventional fronts), and according to which of lows A, B, C or D was considered to be the 'parent' low.

The persistence of C_A and its cloud band are particularly surprising given that the orientation of the temperature gradient noted in (i) above should have rendered the front highly frontolytic[1]. This perhaps implies that differential sea surface fluxes and differential latent heating (as in 'convective frontogenesis', Parker and Thorpe (1994)) had a large and counteracting frontogenetic effect. Latent heating would have been greatest on the southwestern (warm) side of the front, where the deepest convection was occurring, whilst heating by sea surface fluxes may also have been greater on this side, on account of the stronger winds. The existence of a 'warm tongue' immediately ahead of the front (see (ii) and (iii) above) supports this inference.

Figure 5 provided vital additional information for our surface analysis, for 12th/12UTC, in Fig. 6, particularly in the area between Iceland and northwest Scotland where there were just two ship reports. Consider the segment of the trough-line near 62°N, 13°W where there are three adjacent black circles. Wind speeds on either side of this are about 18 and 21ms^{-1}. With a geostrophic assumption this difference constrains the angle between isobars and trough line on the strong wind side to be less than 59° (Eq. (A2) in appendix III). The angle represented on Fig. 6 is 45°. Note also that there is good general agreement between isobaric spacing and SSM/I wind speed around low A, and along C_A. The positive impact of incorporating the SSM/I data can be seen by comparing Fig. 6 with the top right panel of Fig. 2, which would have been drawn without this data. On Fig. 2 the trough line is indistinct and incorrectly oriented, and low A is located too far east.

Figure 7 shows 1000-850hPa thicknesses from three of the radiosonde stations on Fig. 1. Lerwick and Thorshavn were generally on the cold side of the trough line, whilst Stornoway, about 400km away, resided mainly on the warm side. Noting that time increases towards the left, it can be seen that low-level baroclinicity across the trough line generally increased with time, reaching a peak value of about 8°C across 400km early on the 14th. This fits the trend in 1000-500hPa thicknesses noted on Fig. 2.

Early on 14th ship 'OUEV' traversed the trough line (between lows C and D). Its observations are shown in Fig. 8; their locations are marked on Fig. 3. There is strong evidence for a front-like feature between the 00 and 03UTC observations (a 90km distance), in temperature change (4°C),

[1] It is straightforward to show that if the value of $\delta T/\delta P$ along a cold front is negative (positive), then there is geostrophic frontolysis (frontogenesis). The opposite is true for a warm front.

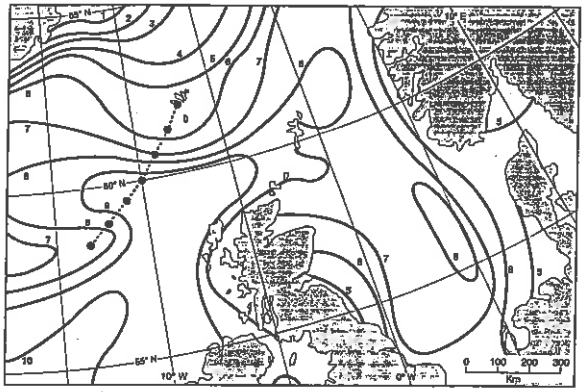

Fig 3: Hand-drawn sea surface temperature analysis for 11-15 March 1992, based primarily on ship reports, but also on LAM grid point values in data sparse regions. Black dots show three-hourly positions of ship 'OUEV', corresponding to the observation sequence in Fig. 8.

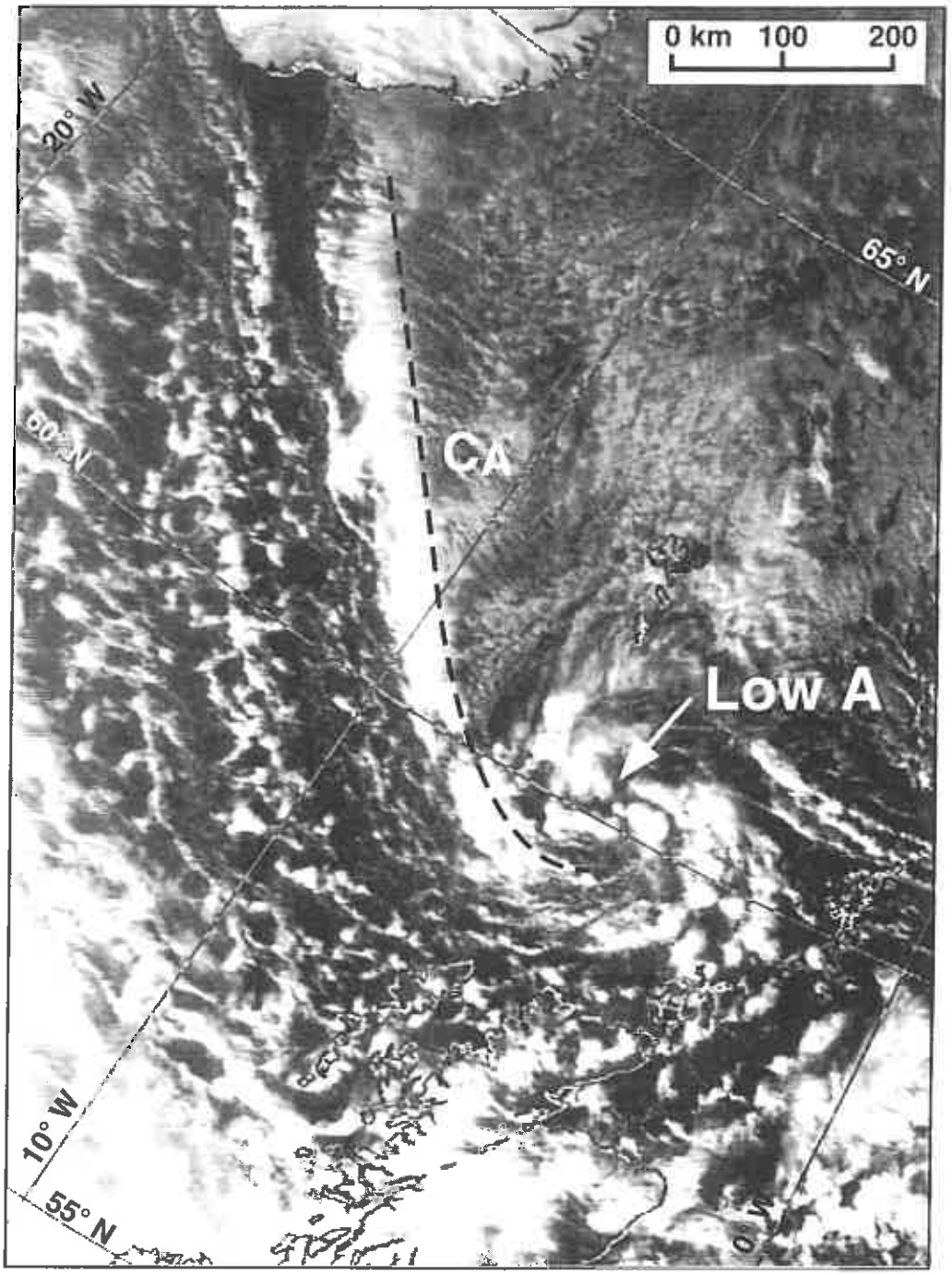

Fig 4: NOAA visible image for 1312UTC on 12 March 1992. The positions, at that time, of polar low 'A' and (mesoscale) cold front C_A are highlighted. Photograph courtesy of the University of Dundee.

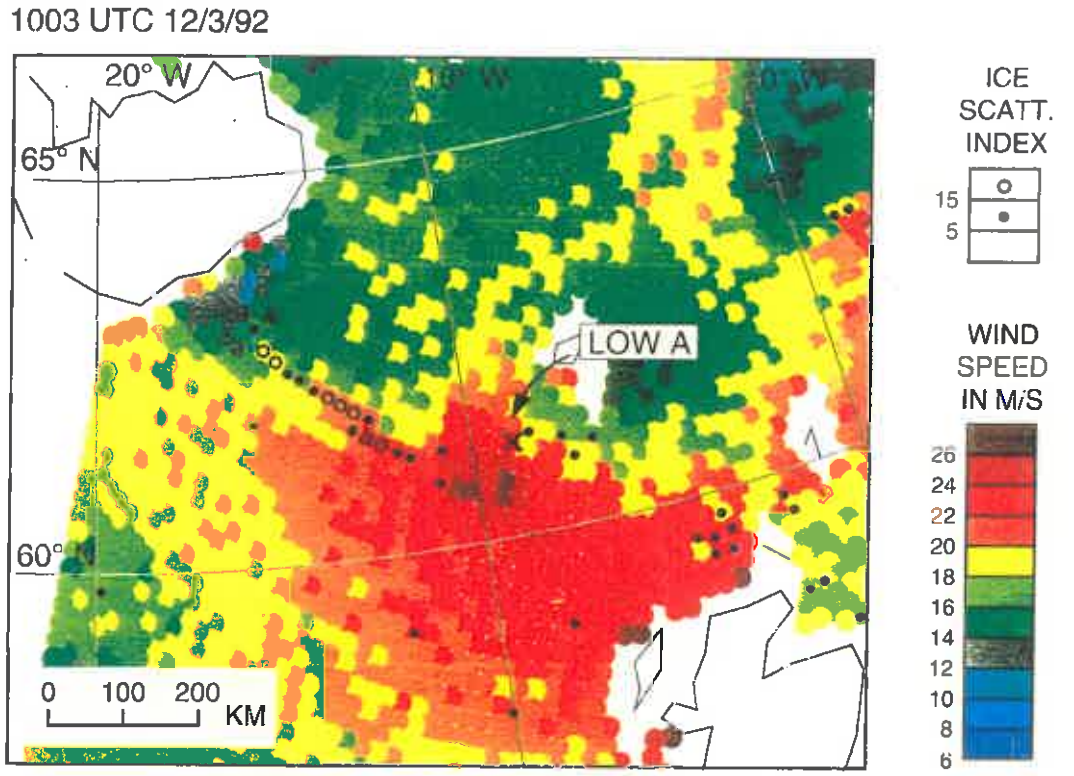

Fig 5: Composited image of SSM/I data for 1003UTC on 12 March 1992. Colours represent surface wind speed in ms^{-1}; symbols show where ice scattering index is greater than 5 (see keys).

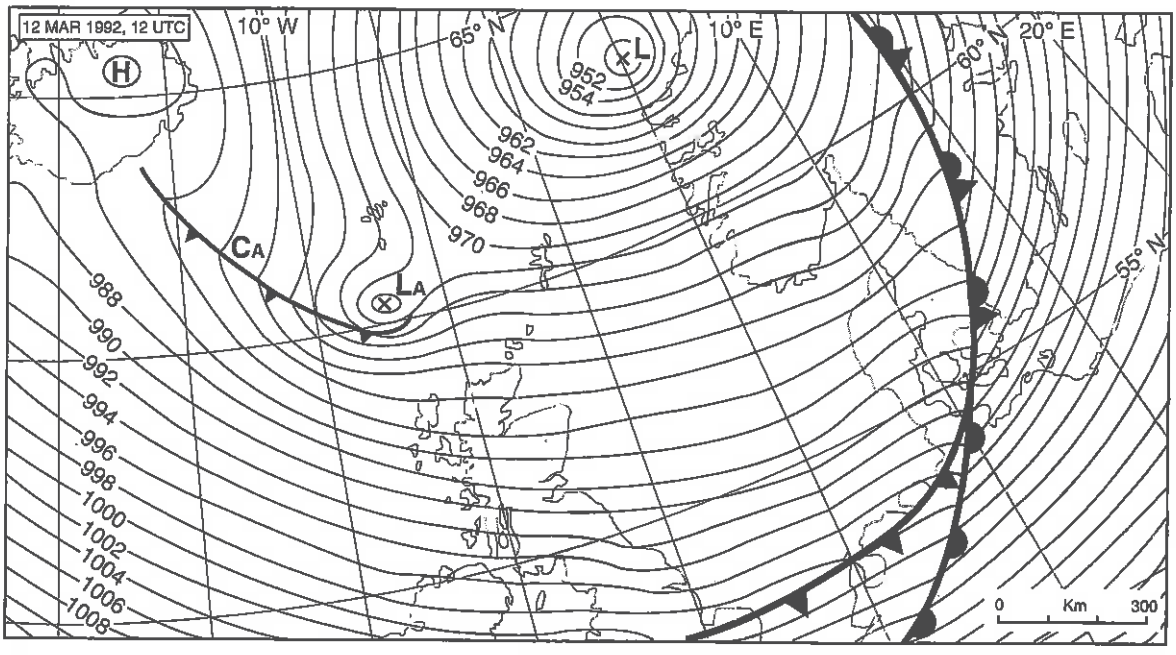

Fig 6: Re-analysed surface chart for 12UTC on 12 March 1992, highlighting polar low 'A' and (mesoscale) cold front C_A.

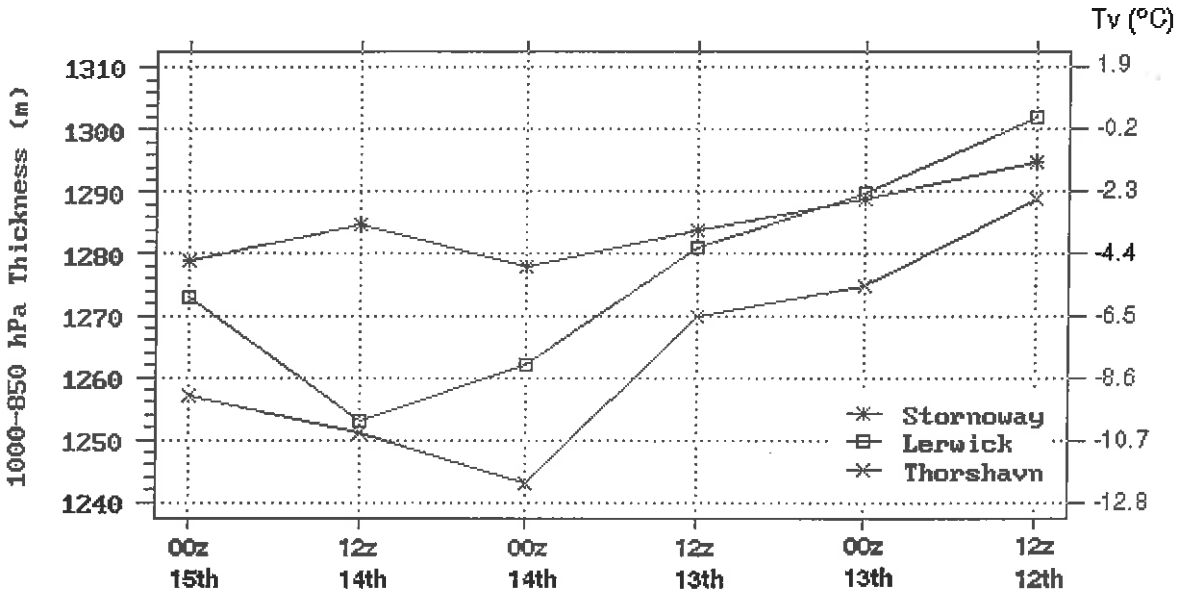

Fig 7: 1000-850hPa thicknesses (m) from radiosonde ascents at Stornoway, Lerwick and Thorshavn (Fig. 1) during the polar low outbreak. Corresponding mean virtual temperature of the 1000-850hPa layer is given by the right hand axis. Time increases towards the left.

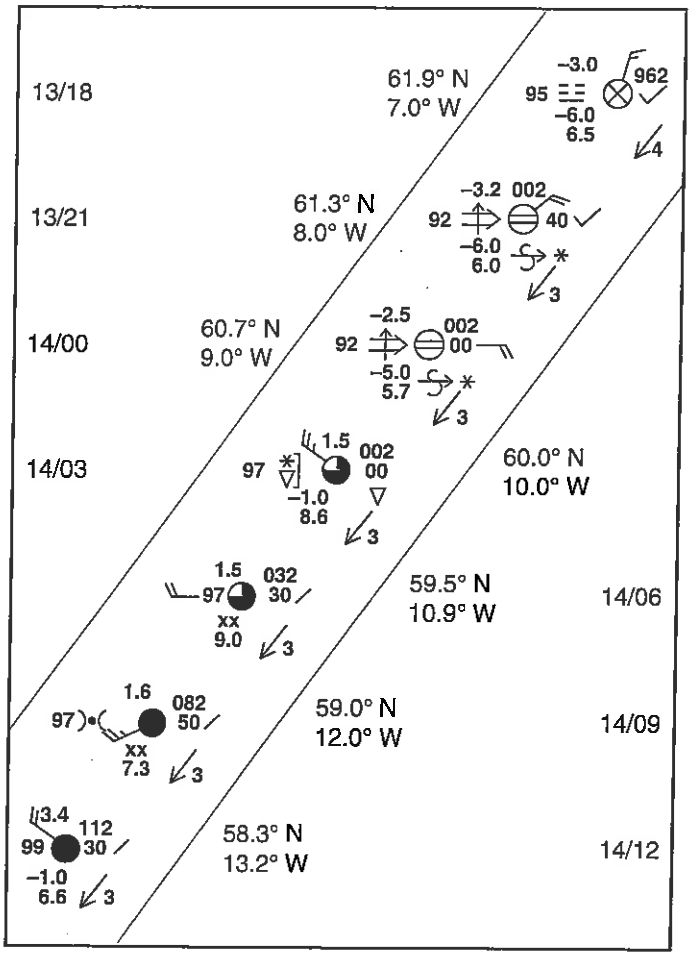

Fig 8: Station circle plots for ship 'OUEV' during its southwestward passage from the Faeroes. Given alongside are time of observation (date/UTC time) and ship location (Fig. 3 depicts these locations).

Tracks of Polar Lows

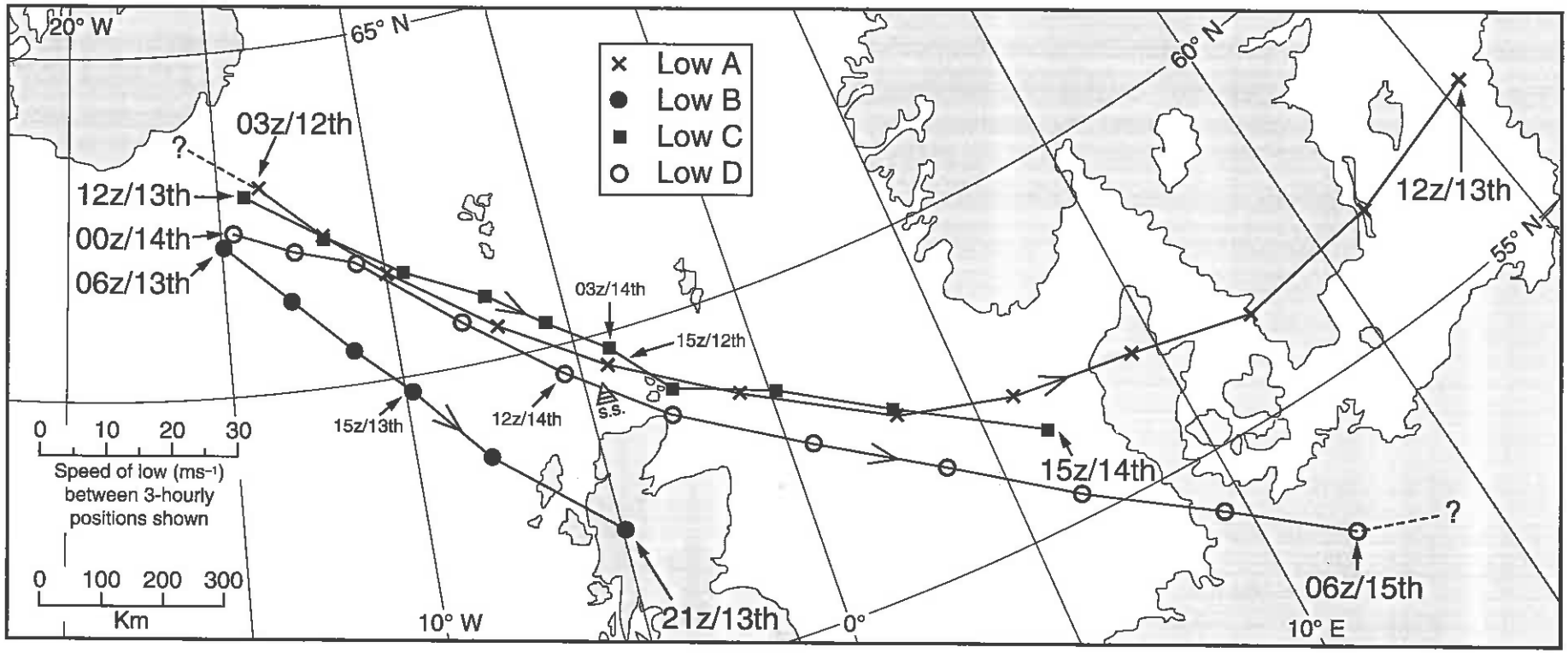

Fig 9: Tracks of the four polar lows. Symbols show positions of the low centres at 3-hourly intervals (see key). Low speed can be deduced using the top scale. Small triangle labelled 'S.S.' represents Sule Skerry (its observations are shown in Fig. 11).

dewpoint change (4°C) and surface vorticity (as represented by a wind shift from 20 knot easterly to 25 knot northwesterly). Wind shifts of such large magnitude are very rarely observed across fronts over the U.K. Figure 7 also provides evidence of some homogeneity in air mass characteristics on either side of the trough line.

To summarise, between 12th and 14th March 1992 four polar lows developed between Iceland and Scotland, on the southwestern flank of the axis an outbreak of exceptionally cold arctic air. A quasi-permanent trough line first appeared in the wake of low A, and it was on this that lows B, C and D all subsequently formed. The trough line had front-like temperature and vorticity signatures, both of which became more prominent with time, in parallel with increasing tropospheric baroclinicity.

5. Evolution and mesoscale features of the four polar lows

Figures 9 to 12 relate directly to the surface analyses, and are referred to extensively in this section. First we present some background information on them.

Figure 9 shows the track of each polar low, whilst Fig. 10a depicts surface analyses at 6-hourly intervals for lows B, C and D. Large symbols denote classical fronts, and small symbols 'meso-' or 'mesoscale' fronts.

Figure 11 shows sequences of observations from Sule Skerry automatic weather station, which lies 16m above sea level on an isolated rocky outcrop 50km north of mainland Scotland (Fig. 1). This station was chosen for its close proximity to the tracks of three of the lows (Fig. 9, marked 'S.S.'), and for the completeness of its observational record. It details well weather fluctuations during the passage of the lows and their fronts. Some caution is required in interpreting the temperature record, for reasons given in Appendix II.

Radar data from the Beacon Hill site is presented in Fig. 12, with surface winds superimposed. In this way the two most prominent identifying characteristics of mesoscale fronts - banded convective precipitation and a strong vorticity signature, or wind shift - have been combined on one diagram. This superimposition proved to be a very valuable aid during the analysis - previously there had been little reason, or intention, to analyse fronts around the polar lows. Note that pronounced convective banding also occurred in regions where there was no surface wind shift, such as between 12 and 18UTC on 13th (bands oriented north-northeastwards), and that such bands have not been analysed as mesoscale fronts or troughs.

a) Low A

i) General evolution

Low A first developed close to Iceland late on 11th or early on 12th, to the west of a large mid-latitude low which was then moving steadily east (at 63°N, 5°E on Fig. 6). By 03UTC there was a well-defined hook or comma cloud associated with the low A, but by 09UTC on 12th this had broken up into spirals of convective cloud (as on fig 4), characteristics which persisted, on Meteosat imagery, for the remainder of its lifetime. Although cold front C_A had a narrow tongue of warm air ahead of it, there was little large scale baroclinicity across the low, Fig. 7 showing (virtual) temperature gradients at 12th/12UTC of just 1°C across 400km. Thus low A can be categorised, perhaps, as a classical convective polar low.

The low tracked southeast then east, at a mean speed of 19ms^{-1} (Fig. 9), weakening only when it crossed southern Sweden on 13th. Here heat and moisture fluxes from the surface would have been considerably reduced, cutting off the energy source for the convection. Up until this period of decay, ζ_g at the low centre had been substantial, of order 10f.

ii) Weather

The passage of low A gave rise to heavy showers of snow, sleet and hail. The most notable weather feature was the wind; maximum speeds occurring just prior to passage of C_A. At Sule Skerry the mean speed reached 54 knots, with gusts to 75 (fig 11), values which were as high as any at Sule Skerry during the polar low outbreak. The SSM/I wind speeds on Fig. 5, although measured 5 hours earlier, give good indication of the relative location of maximum winds (just southwest of the low), as well as absolute values (dark red ~ 27 ms^{-1} ~ 54 knots).

The (area of) strong winds persisted. The large pressure gradient just south of low A at 06UTC on 13th (Fig. 10a) equates to a geostrophic speed in excess of 120 knots, and measured mean surface winds of 50 knots.

b) Low B

i) General evolution

Low B was reasonably well forecast by the LAM (compare 13th/18UTC frames on Fig. 10). Other products from the LAM suggested that it appeared early on 13th in response to the arrival of an upper level trough, or PV anomaly. Simultaneously a band of convective cloud developed eastwards from the low centre - marked as frontogenetic cold front C_B at 13th/06UTC on Fig. 10a. Note that the splaying out, towards the south, of isobars just north of this front (06, 12 and 18 UTC frames) represents a classical frontogenetic deformation pattern.

The NOAA infra-red image for 1317UTC on the 13th in Fig. 13 shows the hook of convective cloud, associated with C_B, winding itself around a clear region coinciding with the low centre. The low remained a relatively weak feature, ζ_g being generally less than for any of the other lows (between about 1f and 2.5f). Had the low developed more the front marked C_B, which is in a rather unconventional location, would have had to move north instead of south.

The surface features and upper trough translated southeastwards towards mainland Scotland at about $15ms^{-1}$. The surface features intensified initially, but then decayed rapidly over land (Fig. 10a).

ii) Cold front C_B

On the afternoon of 13th the convective cells behind C_B appeared, on Meteosat imagery, to join together, producing a layer of stratiform cloud by about 18UTC. Surface observations indicated this to be altostratus. In addition the SSM/I scattering index image for 1922UTC (not shown) suggested that at that time only the southern edge of the precipitation behind C_B (see 1900 to 2100 frames on Fig. 12) was convective. It may be that the altostratus and non-convective precipitation were symptoms of slantwise ascent caused by the upper level forcing evident on the LAM data.

Between 1900 and 2000UTC cells within the cold front precipitation band were moving on a trajectory from about 020° at 22 knots, whilst reported surface winds were about 040°/20 knots. This indicates cold advection, of order 14°C/day (see section 3(b)), which is consistent with the analysis of cold front C_B.

iii) Weather

A broad 120km-wide region around the low centre was generally characterised by light winds and suppressed convection, although a spiral of showers did wind their way into the low centre at later times (see 18UTC frame on 13th on Fig. 12).

As suggested by the pressure gradients on Fig. 10a winds were strongest west of the low centre, ships reporting mean speeds up to 45 knots.

With passage of the cold front temperatures dropped by 1 to 2 deg C, winds picked up to a 20 knot northeasterly, and snow began. The band of snow was approximately 80km wide, and produced a total D_R = 2mm (or Ds = 2.5cm) on the north coast of mainland Scotland. Cape Wrath reported 5cm of fresh (albeit uneven) snow. The snow apparently died out completely after a 100km passage across land (Fig. 12).

After the cessation of precipitation behind C_B the air dried out considerably, dewpoint depressions registered at Sule Skerry between 21 and 00UTC being the lowest in its observation sequence (Fig. 11). This drying may have been due to a combination of slantwise descent below the frontal surface of C_B, and descent induced by the anticyclonic col ahead of low C on the 14th/00UTC frame on Fig. 10a (oriented north-south, around 3°W).

c) Low C

i) General evolution

Low C appears to have developed close to Iceland around 13th/12UTC (Fig. 10a). Icelandic synoptic observations suggested that during the previous 6 hours a surface trough (depicted at 06UTC) had translated southwestwards along the coast, and this may have contributed to the development of the low and/or its cold front Cc. The LAM failed to accurately predict the development or evolution of low C; this could be attributed to an anomaly in its upper level fields which observational analysis suggested was very probably spurious.

Low C translated in an east-southeasterly direction at about $12ms^{-1}$ (Fig. 9), until passing over Orkney around 06UTC on 14th (Fig. 14 shows a NOAA infra-red image close to this time). ζ_g at the low centre was then near to its peak value of about 3.5f. However at no time did the low exhibit any marked intensification.

The frontal positions shown on Fig. 10a are more akin to those belonging to classical frontal waves than were those of either low A or low B. The length scale is however smaller than for waves which typically form on classical fronts, by perhaps 50%.

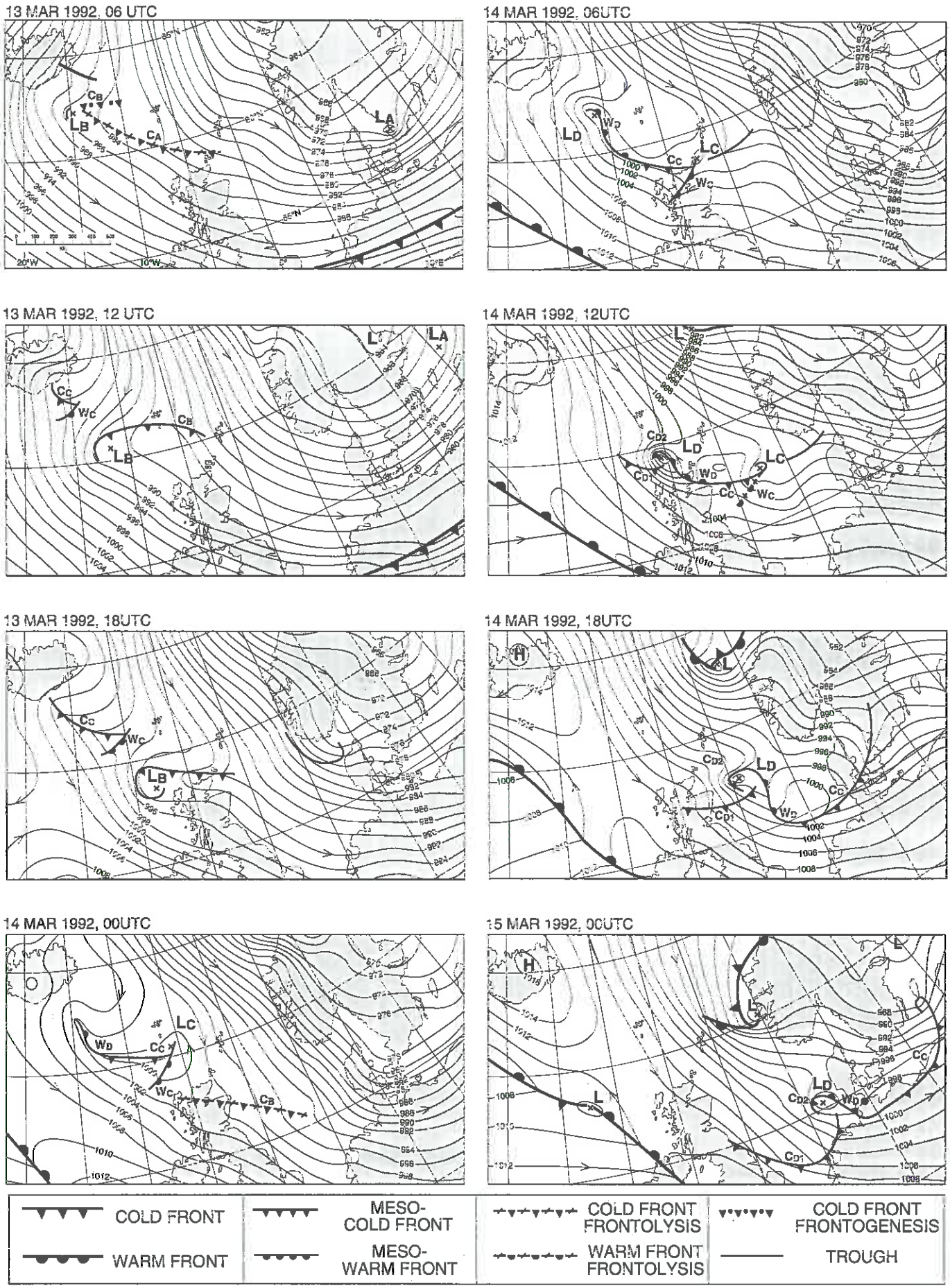

Fig 10a: Sequence of re-analysed surface synoptic charts, at 6 hourly intervals from 06UTC on 13 March 1992 to 00UTC on 15 March 1992 (2hPa isobar interval). Distinction is made between 'mesoscale' fronts (small symbols) and classical fronts (large symbols) (see key and text). Mesoscale fronts are named according to parent polar low (eg warm front Wc and cold front Cc belong to low C). Black dot on final panel is the position of Schleswig (see Fig. 19).

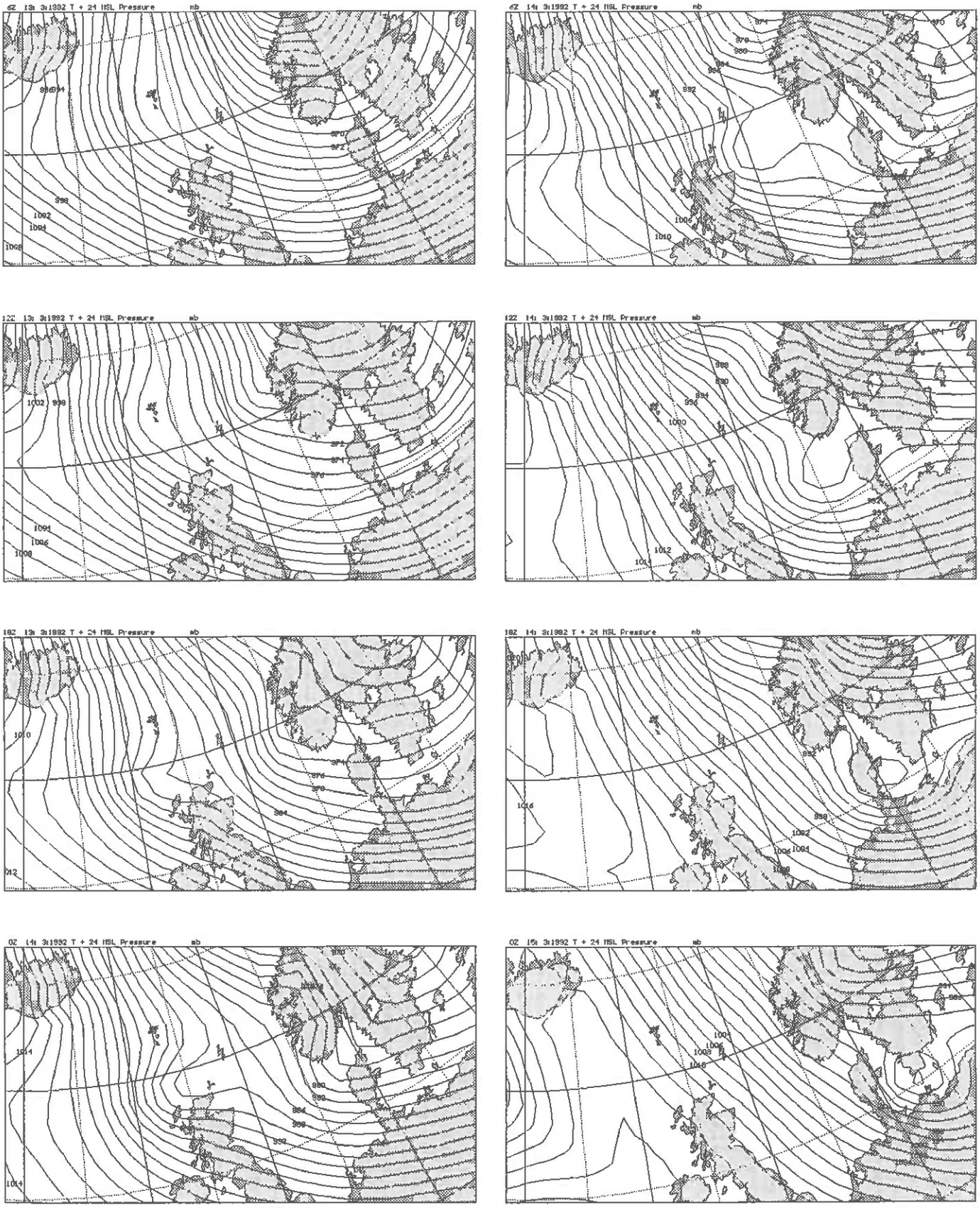

Fig 10b: Sequence of 24-hour forecast charts taken directly from the UK Met Office LAM, for times at 6 hourly intervals between 06UTC on 13 March 1992 and 00UTC on 15 March 1992 (2hPa isobar interval). Panels are laid out as on Fig. 10a, to facilitate comparison.

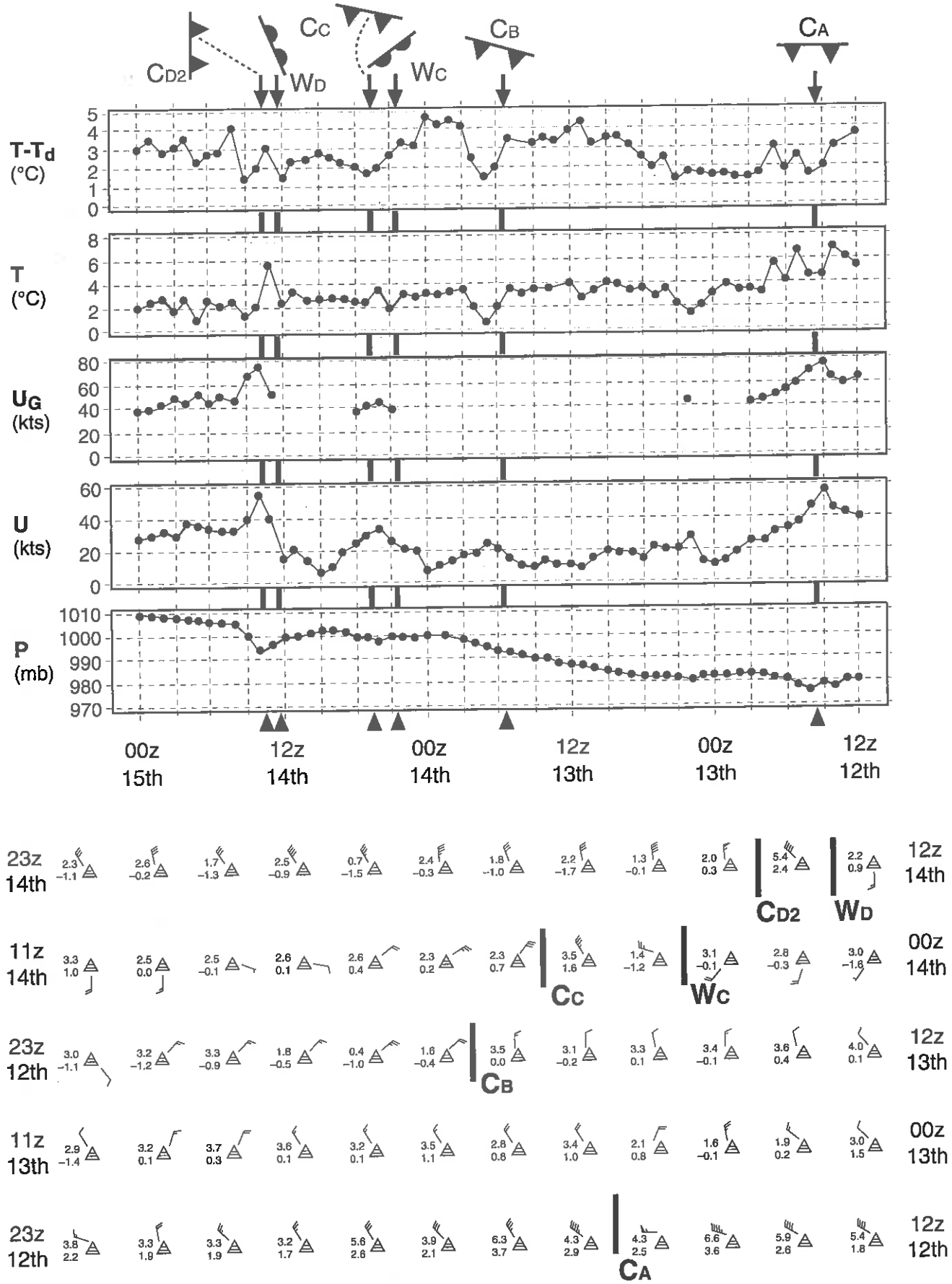

Fig 11: Hourly observations from Sule Skerry automatic weather station for 12UTC, 12 March 1992 to 00UTC, 15th. T-T_d is dewpoint depression, T temperature, U_G maximum gust during previous hour (only reported when > 35 knots), U wind speed (mean over the 10 minutes leading up to observation time) and P mean sea level pressure. Wind directions are shown in lower part of figure (these plots also give wind speed (full barb = 10knots) and T and T_d (°C)). Time increases from right to left, and from bottom to top on wind plots. Arrows and thick lines denote time of passage of a (mesoscale) front (labelled as on Fig. 10); front orientation at this time is illustrated at top of figure (where north = y axis).

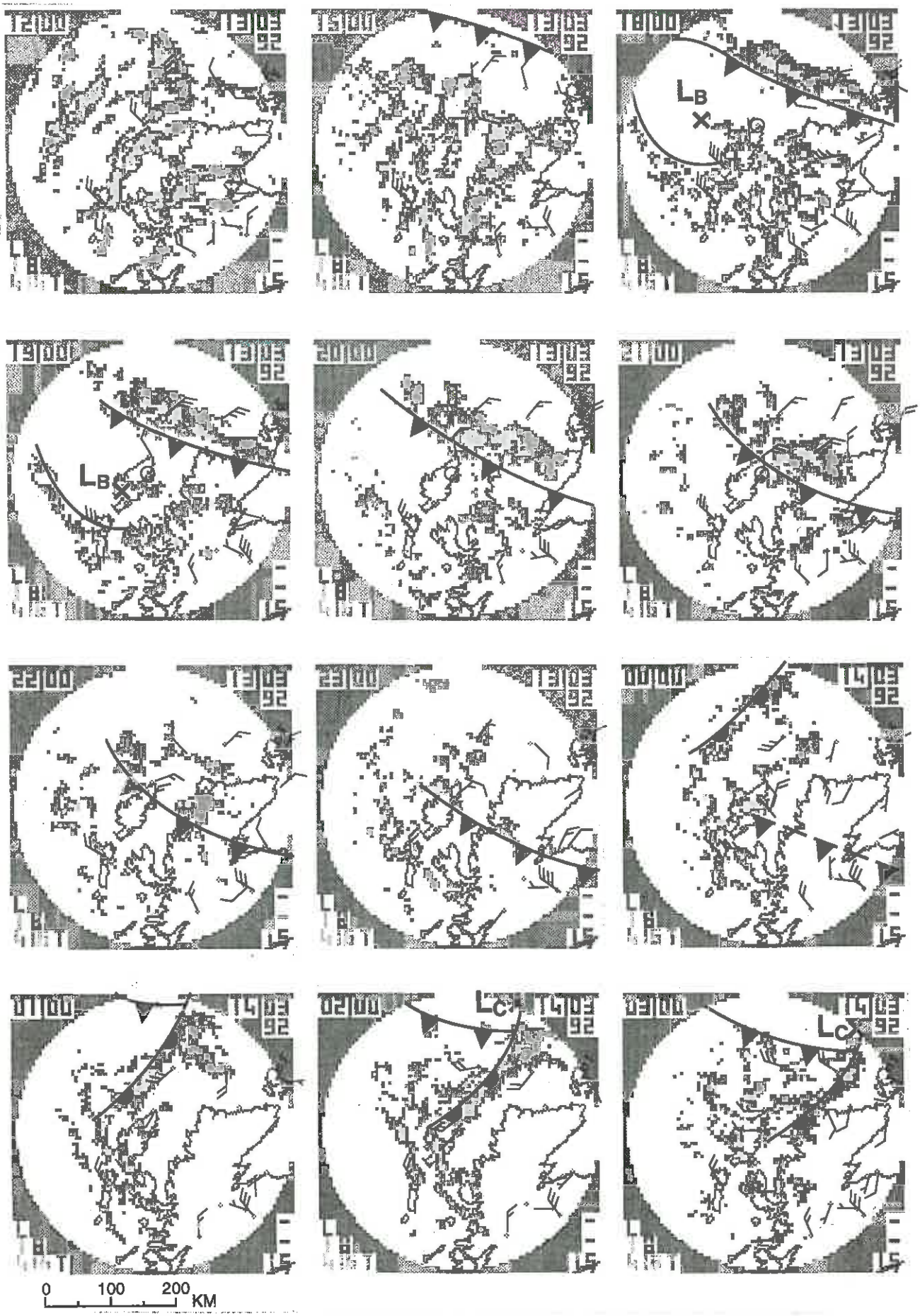

Fig 12: Radar data from Beacon Hill site for 13/14 March 1992. Time is in top left of each panel, date in top right. Rainrate conversions (also see lower left of panels) are as follows:
Dark grey ('L'): 0.125 to 1mmhr^{-1} Light grey ('1'): 1 to 4mmhr^{-1} ....
Very few pixels correspond to >4mmhr^{-1} (typically 1 or 2 per panel). Rates assumes rain; (T) columns in table 1 give better guide for snow observed. Surface winds, low centres, and (mesoscale) fronts are also shown. (figure continued on next page)

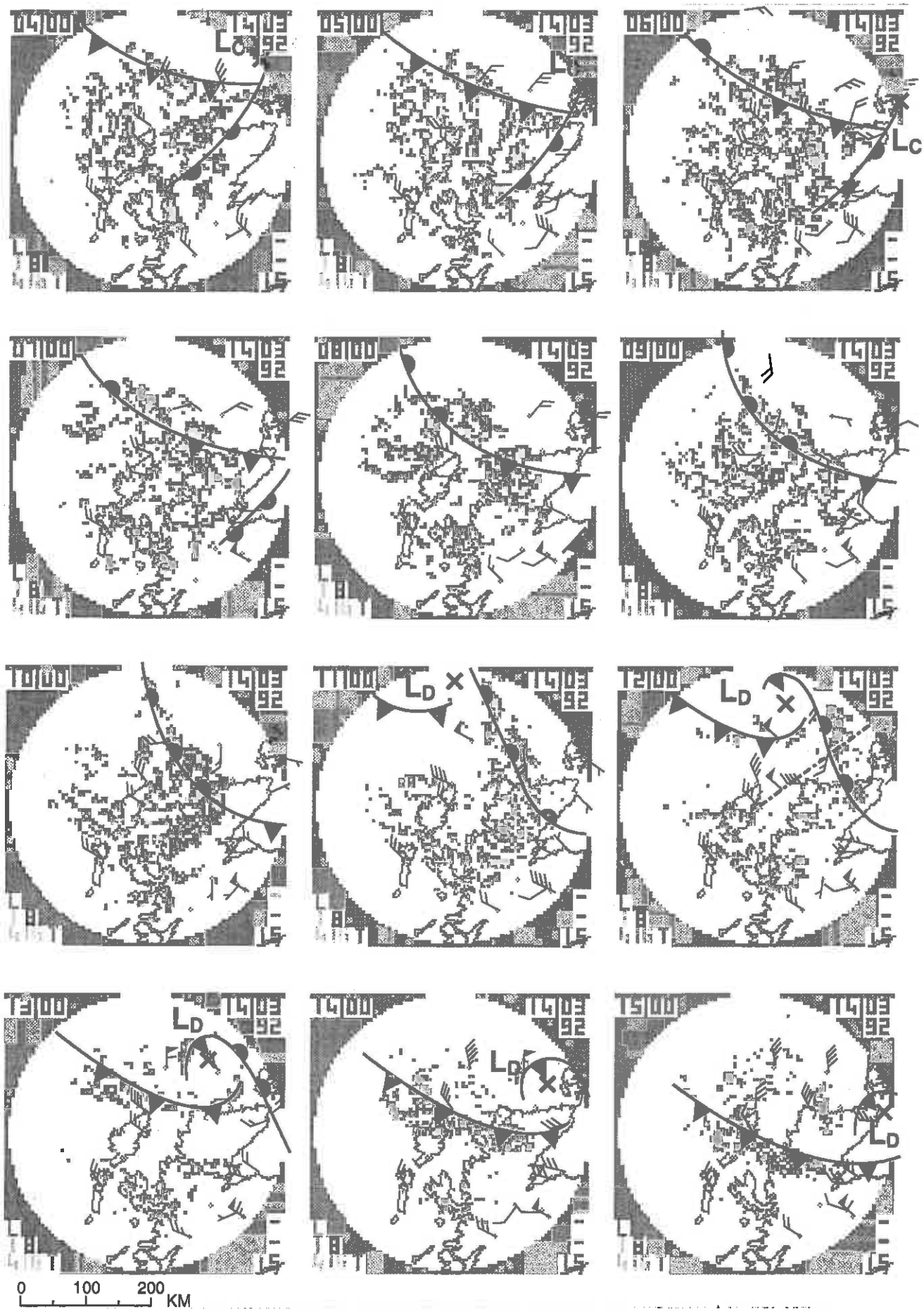

Fig 12 (cont.): Radar data from Beacon Hill site for 13/14 March 1992. Time is in top left of each panel, date in top right. Rainrate conversions (also see lower left of panels) are as follows:

Dark grey ('L'): 0.125 to 1mmhr^{-1} Light grey ('1'): 1 to 4mmhr^{-1} ....

Very few pixels correspond to >4mmhr^{-1} (typically 1-2 per panel). Rates assumes rain; (T) columns in table 1 give better guide for snow observed. Surface winds, low centres, and (mesoscale) fronts are also shown. Dash-dot line on 14th/12UTC frame is location of part of the cross-section in Fig. 22.

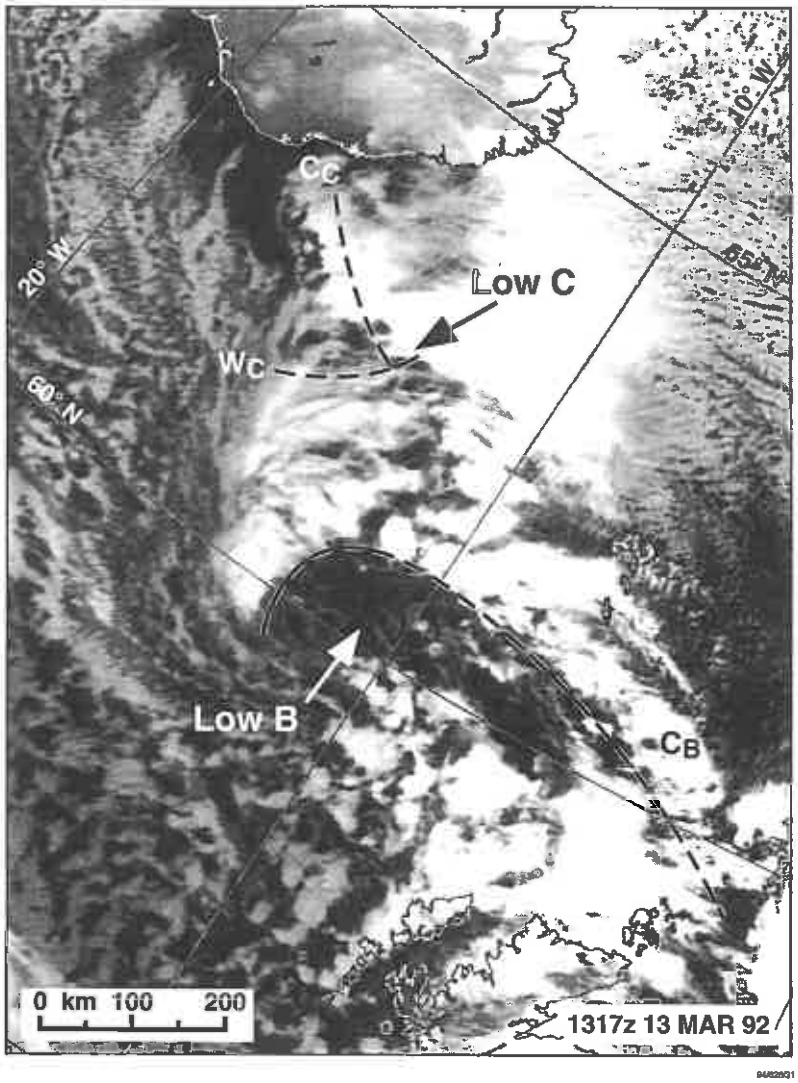

Fig 13: NOAA infra-red image for 1317UTC on 13 March 1992. The positions, at that time, of lows B and C and their respective (mesoscale) fronts are highlighted. Photograph courtesy of the University of Dundee.

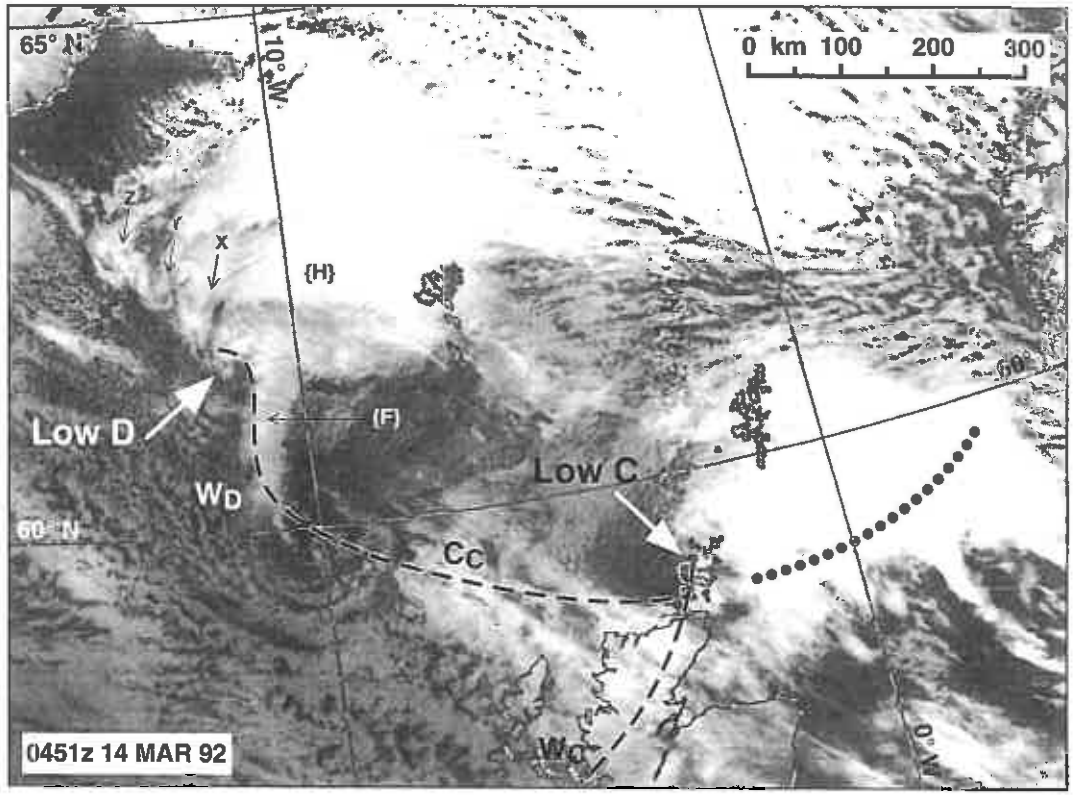

Fig 14: NOAA infra-red image for 0451UTC on 14 March 1992. The positions, at that time, of lows C and D and their respective (mesoscale) fronts are highlighted. The thick dotted line is a surface trough (see Fig. 10). {F} represents a frontal cloud band, {H} the cloud head region, and X, Y and Z three additional cloud features (see text). Photograph courtesy of the University of Dundee.

Between 06 and 15UTC on 14th the low centre, it's fronts and a trough to the east (first shown on the 06UTC frame on Fig. 10a), continued moving east-southeast, but at an increased speed (Figs 9 and 10a). The warm front decayed, as described in 5(b)(ii) below. The low also decayed, *prior* to encountering land. However the cold front persisted until 15th, maintaining a band of convection ahead of it. The trough continued to develop and extend further east, and as the low decayed it effectively joined up with Cc.

Figure 15 displays SSM/I wind speed and scattering index data for the time when low C was decaying and the trough and cold front amalgamating into one. The line of the surface pressure trough is indicated by a linear discontinuity in wind speed, running along about 55.5°N between 1.5°E and 8°E (appendix III). Wind speeds on Fig. 15 were used to aid the surface analyses (Fig. 10a) in the same way that Fig. 5 contributed to the analysis in Fig. 6. For example the wind speed minimum centred around 56°N, 4°E corresponds to the small anticyclone between lows C and D.

ii) Warm front Wc

The first evidence of Wc was provided by 3-hourly observations from ship 'TFLA', located around 62°N, 15°W. Between 12 and 15UTC on 13th its temperatures showed a sudden jump, from -4°C to -1°C, whilst the present weather changed from 'continuous moderate snow', with 50 to 200 metre visibility, to 'moderate/heavy snow shower', with 0.5 to 1km visibility. This transition corresponds to the boundary, on Fig. 13, between a relatively solid cloud mass ahead (southeast) of Wc and fragmented convective cloud behind.

A band of deep convection developed along Wc prior to its movement across Scotland. On the Meteosat sequence the cloud band is initially poorly defined, but after about 1900UTC becomes pronounced, its tops at -40°C corresponding with a height, from soundings, of about 5km. SSM/I data (not shown) indicated that the cloud was convective.

The passage of the front was apparent in temperature and wind observations from Aberdeen (Fig. 1), although frontal precipitation and cloud had disappeared earlier, after a 100 to 150km passage across land.

The lack of coherent individual cells in the convection ahead of Wc when within the area of radar coverage meant that neither cell velocity nor thermal advection could be derived.

iii) Cold front Cc

Cold front Cc was well defined by surface winds and temperatures for about 36 hours - on Fig. 8, on other ship observations (not shown), on Fig. 11, on the 04 to 09UTC frames on Fig 12, on Fig. 15, and on reports from a north sea rig at 56.3°N, 2°E shown on Fig. 17. However it was at times difficult to distinguish Cc on the basis of imagery alone. Although at initiation it coincided with a short line of convective cells (fig 13), by 0455UTC on 14th (Fig. 14) there was a distinct lack of coherence to the cloud structure, particularly around 60°N 10°W. This is consistent with the radar data in Fig. 12, which shows Cc to be characterised by a fragmented band of convective precipitation, found mainly on the warm air side. To the rear of the front convection is heavily suppressed. Note the dark area over and to the west of low C on Fig. 14, suggesting general descent.

In the area just behind Cc where there *were* convective cells they were moving from about 320° at 20 knots, whilst surface winds below were about 040°/15 knots. Thus in the 1000-800hPa layer (see section 4(a)) just behind Cc the thermal wind was about 280°/23knots and the geostrophic thermal advection about -27°C/day. Both are substantial and thus lend weight to the frontal analysis. The thermal wind is also front-parallel.

After passing over Scotland Cc developed a more coherent line of convective cells ahead of its surface position, as shown by the inset on Fig. 15, and imagery on Fig. 17.

iv) The 'warm sector'

Between Wc and Cc is what might be termed a mesoscale warm sector, in which there are widespread convective cells (Fig. 12). This is in marked contrast to the regions beyond the warm and cold front precipitation bands, which were essentially free of convective precipitation. It also contrasts with warm sectors typical of 'standard' marine mid-latitude cyclones. The air in such warm sectors has usually been cooled from below, generating extensive low cloud, drizzle and poor visibilities, and inhibiting convective development.

Movement of cells in the warm sector was not perceptibly different to that of cells just behind Cc, suggesting that they were within the same airmass.

v) The trough

A prominent feature on Fig. 14 is the area of high cloud east of low C. This connects to the surface trough (marked as a line of dots on Fig. 14) which first became evident between 00 and 03UTC

on 14th. Within a short time this trough became very active, giving rise to a 90 degree wind shift at the surface by 06UTC (note the isobars on Fig. 10a) and showing up as a solid 100km wide band of vigorous convection on the next SSM/I scattering index image (for 0901UTC, not shown). Signs of trough development can perhaps be seen at 01 and 02UTC on Fig. 12, in the area southeast of the triple point. Note however that this would be just the tail end - on the SSM/I image the convection is centred 200km east-southeast of low C.

The trough-line was analysed as a trough and not as a mesoscale front on the basis of reported surface temperatures and the fact that it was some distance from the main mesoscale frontal zone. However this evidence was not considered particularly conclusive. The sudden appearance of the feature, its location, its convective nature and the fact that cloud top temperatures were coldest at its northeastern end suggest that it could be analogous to a type I instant occlusion (see Mcginnigle (1990) and Browning and Hill (1985)).

The sudden development occurred where there was good data coverage, and was investigated further. It appears that development could be related to a subtle change in the characteristics of the pressure pattern in the area immediately east of low C. An anticyclonic col centred at 60°N 3°W at 00UTC (Fig. 10a), which probably produced divergence at the surface (see section 5(b)(iii)), had by 03UTC converted to a neutral or cyclonic col, both of which would produce convergence at the surface. In a very unstable atmosphere a small localised area of convergence could easily be sufficient to trigger organised convection. The anticyclonic col had been a legacy of the circulation around low B, and probably disappeared as low B decayed over land.

A second and perhaps more important factor relates to winds over northern Scotland. Towards the eastern edge of the 03UTC frame in Fig. 12 these are generally southerly. Most of this flow is cross-isobaric, partly because the surface winds have backed in response to stabilisation caused by night-time cooling over land (for most of the polar low outbreak cross-isobaric wind components were very small, as expected in generally unstable conditions). Such a large cross-isobaric component would contribute greatly to any surface convergence apparent east of low C in the area where the trough was rapidly developing. Indeed the 2-dimensional divergence at 03UTC between Kirkwall and Sumburgh, (evaluated along a 130km line between them, see Fig. 1) was a substantial $-11 \times 10^{-4} s^{-1}$.

Whilst the above inferences are difficult to verify, they do give an example of how development of synoptic scale features in an unstable airmass can potentially depend on a complex interplay between many factors; such as the evolution of the background synoptic pattern, the influence of sea surface fluxes on features within this pattern, the land/sea distribution, and the diurnal heating cycle over land (see Pike (1990a and b) for further examples of such effects). It is to be expected that such interplay would present difficulties for numerical models, and this may partly explain why the detail of the forecasts in Fig. 10b is so poor

vi) Weather: precipitation

As warm front Wc approached northwest Scotland it was associated, on its 'cold air' side, with a coherent 30km wide band of convective snow, in which R locally exceeded $4 mm hr^{-1}$. The precipitation died out after about a 150km passage across land. By contrast snowfall along cold front Cc was considerably more fragmented and of slightly lower intensity. It was still convective in nature but the cells translated *along* the front.

Radar data from the Beacon hill site suggested that Wc produced D_R = 0.9mm (or Ds = 1.1cm) across northwest Scotland, snow duration being about 0.75 hours. Thereafter 6 hours of convective precipitation in the warm sector (0230 to 0830UTC) generated a total D_R = 1.5mm (or Ds = 1.9cm). Totals for Cc were difficult to estimate, but were probably of order D_R = 0.8mm (Ds = 1cm) over 3 hours. This represents the same rate as for the convection within the warm sector.

The heaviest area of precipitation was associated with the trough east of the low centre. This was most active outside the radar area. At Fair Isle 15cm of (drifting) snow accumulated between 00 and 06UTC in connection with the trough's passage, whereas at Sumburgh, 40 km upstream, the accumulation during this time was only 1cm. This re-emphasises the sudden appearance of the trough line described above in sub-section (v).

vii) Weather: miscellaneous

Figure 11 shows a pressure drop of about 2hPa during the passage of low C. It also shows that the area of strongest winds (means of 25 to 35 knots) straddled the cold front (also see Fig. 12). Close to the low track maximum reported gusts were between 40 and 55 knots. Temperatures generally reached their peak values just ahead of the cold front (as they did with C_A), the perturbation being about 1°C. Further from the low centre, at Stornoway and Butt of Lewis, passage of the warm front brought a sustained temperature rise of 1 to 3 deg C. This is consistent with Fig. 8, on which

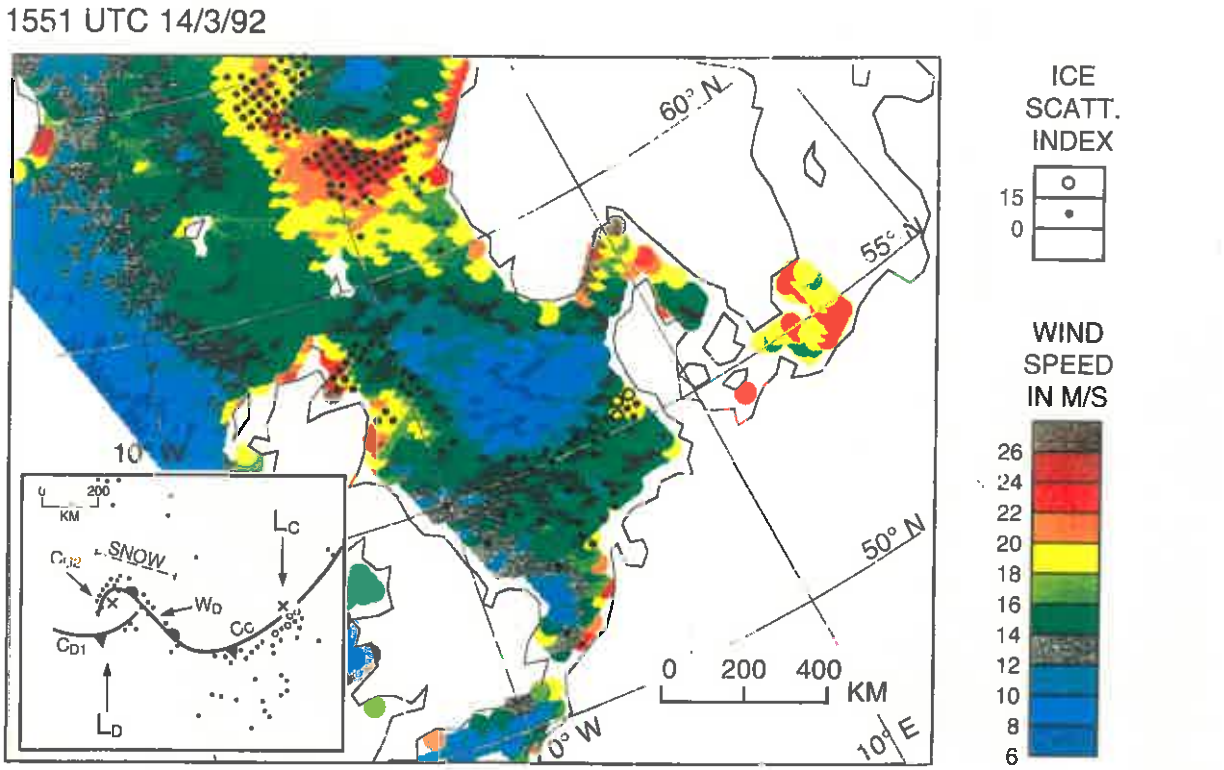

Fig 15: Main figure: composited image of SSM/I data for 1551UTC on 14 March 1992. Colours represent surface wind speed in ms^{-1}; symbols show where ice scattering index was non-zero (see keys). **Inset**: Scattering index symbols from main figure plotted in relation to simultaneous positions of (meso-) synoptic features (labelling as on Fig. 10). 'SNOW' axis corresponds to the system-relative position of 5 to 6 hours of moderate/heavy snow reported from Fair Isle.

the virtual temperature of the 1000-850hPa layer at Stornoway increases by about 2 deg C between 00 and 12UTC on 14th.

d) Low D

i) General evolution

Low D first developed late on 13th at the tail end of cold front Cc, over seas just southeast of Iceland. Between 15 and 21UTC on 13th Cc had remained virtually stationary in this area, in spite of there having been a pressure gradient acting to translate it southwestwards. The appearance of low D was signified on Meteosat imagery by an *eastward* translation of the frontal cloud (now of warm front W_D), and the development of a tiny hook at its northwestern limit. These features only became visible at 02UTC; between 21 and 23UTC banded upper level cirrus had obscured surface features, and the 00 and 01UTC frames were missing. The hook and cloud band (marked '{F}' for frontal cloud) show up clearly on the NOAA image for 0451UTC on 14th (Fig. 14).

The period from 00 to 12UTC on 14th was characterised by considerable development of low D as it approached northern Scotland (Fig. 9). Between 00 and 06UTC the low moved east-southeast at $10ms^{-1}$ and deepened from 1001 to 998hPa, ζ_g at its centre increasing from 5f to 8f. From 06 to 12UTC the low moved more rapidly, at $18ms^{-1}$, towards the southeast, deepening to 993hPa as ζ_g increased to a remarkable 15f. By comparison the relative vorticity ζ at 12UTC was just 5f, illustrating the large impact of curvature in reducing wind speed. Nevertheless 5f is still substantial, being greater, by 25%, than that found by Gyakum (1983) at the centre of the 'QEII storm'.

Low D attained maximum intensity around 14UTC on 14th. This was the time at which the lowest station pressure was reported - ie 993.5hPa at Sule Skerry (Fig. 11). Early in the polar low outbreak pressure readings from Sule Skerry were not obviously in error, but by late on 14th they were clearly 1 to 2mb *too high* compared to surrounding observations. If this error was present at 14UTC on 14th, which seems likely, the true pressure then should have been about 992hPa, which implies, in conjunction with other observations, that the minimum pressure attained by low D (around 14UTC) was 990 or 991hPa. In turn this gives a maximum 6-hourly deepening for the low of 6hPa.

To further assess the 'severity' of low D we have estimated a value for the 'maximum geostrophic gradient' within its circulation. This probably occurred west of the centre around 14UTC. At this time the pressure difference between North Rona and Sule Skerry (allowing for the error indicated above) was 10.8hPa, giving a geostrophic wind speed of 160knots (across 80km). This is substantial. By comparison the maximum geostrophic wind within the 'October storm' of 1987 (across 80km) was 210knots (Meteorological Office, 1987, from their analysed U.K. hourly charts).

Several data sources suggest that the rapid development of low D occurred *in the absence of perceptible upper level forcing*. This is the subject of ongoing investigations.

Figure 14 shows three other noteworthy cloud features northwest of low D; a second 'hook' (labelled X) and what appear to be two tiny vortices (labelled Y and Z). Immediately southwest of these features there is a narrow 20 to 60km wide darker band, indicating suppressed convection. The next NOAA image, for 0810UTC (not shown), indicates the area of suppressed convection and remnants of X, Y and Z to be propagating southwards west of the low centre. It was amongst the remnants of X, Y and Z that cold front C_{D1} formed, being first identifiable as a coherent linear structure on the 11UTC Meteosat image. The area of suppressed convection was similarly maintained; it can be seen ahead of C_{D1} on the 11 to 15UTC frames for 14th on Fig. 12.

At 12UTC on 14th low D possessed a cold front C_{D1}, a warm front W_D, and a bent back extension of this warm front, marked as cold front C_{D2} (Fig. 10a). This picture is very similar to the 'T-bone' phase in Shapiro and Keyser's (1990) definition of the life cycle of a rapidly developing mid-latitude cyclone. However low D's dimensions are about 80% smaller than those of the examples they present. Although cold front C_{D1} seemed to develop southwest of the low centre around 11UTC, the way in which it formed from cloud features which were initially northwest of the low centre on Fig. 14 could be thought of as being analogous to the 'frontal fracture' process which precedes the T-bone phase in the Shapiro/Keyser model.

Between 12 and 21UTC on 14th low D continue to move southeastwards, at $21ms^{-1}$, and steadily weakened, ζ_g by 21UTC being 6f. The T-bone frontal structure was essentially maintained, suggesting that the final warm-core seclusion phase in the Shapiro/Keyser model was not wholly replicated. However there were indications of a warm core at the time of maximum intensity; this is illustrated in section 6.

A feature that low D did show which is more prominent than in the Shapiro/Keyser model was a very tight pressure gradient *immediately* northwest of the low centre. On Fig. 10a this shows up particularly well on the 18UTC frame (an analysis supported by 4 ship observations within 50 km of the centre). The fact that the time of minimum pressure on Fig. 11 (14UTC) peculiarly coincides with the (northerly) wind maximum is further evidence.

From 21UTC on 14th to 06UTC on 15th low C continued moving southeastwards, at 21ms^{-1}, crossing the coast of northern Germany around 02UTC. In spite of passing over land the low's intensity was maintained, ζ_g at 06UTC being 6f. The evolution beyond 06UTC has not been the subject of this study. However operational charts do suggest that on 16th the low re-developed markedly between 25°E and 30°E, this time seemingly as a result of upper level forcing.

ii) Warm front W_D

Throughout the phases of low D's life cycle investigated for this paper W_D remained an active feature, being characterised by a strong vorticity signature (as shown by the winds on the 08 to 13UTC frames on Fig. 12) and a narrow but prominent band of precipitating, convective cloud (figs. 12 and 14). The inset on Fig. 15 supports the assertion that precipitation along W_D, and indeed along C_{D1} and C_{D2}, was convective.

On Fig. 14 streaks of upper level cirrus can be detected running northwest - southeast into mainland Scotland. These are high up in the troposphere within a tropical maritime air mass which reaches the surface at the classical warm front seen in the southwest of the later frames on Fig. 10a. Between 02 and 06UTC on 14th Meteosat imagery showed there to be a very clear break in this cirrus, immediately ahead of the cloud band linked to W_D, and moving at precisely the same speed as this cloud band (it is apparent, though less obvious, on Fig. 14). The break may represent cirrus evaporation caused by slight local descent. However this curious feature requires further investigation. After 06UTC on 14th the cirrus streaks were less prominent, and generally located southwest of W_C.

Between 10 and 12UTC on 14th precipitation cells ahead of Wc had a trajectory from 290° at 33 knots, whilst the surface winds were about 180°/16knots. This gives a substantial thermal wind of 310°/41knots, and a geostrophic temperature advection of +45 deg C/day (see section 4(a)). Both support the analysis of a warm front.

iii) Cold front C_{D1}

The initiation of C_{D1} around 11UTC on 14th was discussed above in sub-section (i) in the context of the general evolution of low D. Subsequently the front moved rapidly southeastwards in strong winds on the western flank of the low (Fig. 10a).

Passage of C_{D1} was marked by a wind veer of about 30 degrees, preceded by a narrow band of fragmented convective precipitation (14th/12 to 15UTC frames on Fig. 12, and Fig. 15). Additional data, to be presented in section 6, shows that the convection was being capped by an inversion between about 2.5 and 4.5 km. This inversion is the frontal surface of the classical warm front referred to above in sub-section(ii).

Precipitation cells seemed to be moving with the surface winds, probably because they were ahead of the surface front. There may still have been cold advection at the front.

Both radar data and CTTs from Meteosat imagery suggested some decay of the western end of C_{D1} as it crossed land, although this was less marked than it had been on other (mesoscale) fronts.

iv) Cold front C_{D2}

As indicated in 4(d)(i) above cold front C_{D2} is the bent back extension of warm front W_D. The front was analysed as a cold front on the grounds that it was clearly propagating in a southeasterly direction, and introducing colder air to surface locations. This analysis detail differs from the conceptual model of Shapiro and Keyser (1990) but agrees with analyses shown elsewhere (e.g. Browning and Roberts (1994)).

With time, under the influence of a strong cyclonic circulation, cold front C_{D2} encircles low D (compare the 06, 12 and 18UTC frames on Fig. 10a). The frontal positions shown are based partly on Meteosat imagery, which after 18UTC shows spirals of cloud surrounding the low centre.

v) Weather: precipitation

Precipitation in the vicinity of low D on the radar data (Fig. 12) was mostly confined to regions close to the fronts. Both Wc and C_{D1} were associated with fairly coherent bands of convective precipitation (mainly snow). These bands, about 40km wide, were immediately ahead of the respective surface fronts, and exhibited rates up to about R = 2mmhr^{-1}. At individual locations snow from Wc lasted about 1 hour, giving D_R = 1mm (or Ds = 1.3cm). Conversely snow and hail from C_{D1} lasted about 30 minutes, giving D_R = 0.4mm (or Ds = 0.5cm), the smaller values being mainly due to faster movement of the front.

Figure 12 suggests precipitation on C_{D2} was relatively light, and had a northeastern limit. However this impression is misleading - overshooting was probably a substantial source of error. The inset on Fig. 15 and surface reports of heavy snow showers support this assertion. Meteosat imagery

suggests that the precipitation area on C_{D2} was wedge shaped, so to generalise about duration and amounts would be misleading.

The main area of precipitation associated with low D does not appear on Fig. 12 and has so far not been discussed. This is associated with a 'cloud head' type feature which developed northeast of the low centre from the mass of cloud marked '{H}' (for 'head') on Fig. 14. It will be described extensively in section 6. Surface reports indicate that this cloud head generated as much as 6 hours of continuous moderate or heavy snow. Visibilities taken from these reports can give approximate rainfall equivalents for the observed snow, using an equation in Ludlam (1980, page 356) which relates precipitation rate R, in snow, in $mmhr^{-1}$, to reported visibility V, in km:

$$R = 1.5 / V \qquad (1)$$

Ludlam states that this should be valid for values of R between about 0.2 and $4mmhr^{-1}$, or equivalently values of V between about 8km and 400m. Equation 1 should give a more reliable value of R than converting directly from reported snow intensity, as there is greater resolution in visibility reports. Of the stations on Fig. 1 Fair Isle reported the most persistent snow. Converting its reported visibilities using the above equation, assuming persistence between hourly observations, gives D_R ~ 10mm (or Ds ~ 12.5cm). The validity of Eq. 1 will break down in instances where visibility is impaired by severe drifting. Although drifting was reported from Fair Isle scrutiny of a variety of observations from 14th suggested that its impact on the 6-hour rainfall total derived would have been small. The impact of this drifting on snow depths was probably much greater. The value Ds ~ 12.5cm quoted above corresponded to a period when reported snow depth increased by only 4cm (from 15 to 19cm). Our derived values are considered far more representative.

vi) Weather: miscellaneous

Low D and its fronts show up more clearly on the observations in Fig. 11 than any other low or front, probably because low D was the most intense low. The two main features are the temperature perturbation between fronts Wc and C_{D2} (3 to 4 deg C), and the exceptionally strong winds just to the rear of C_{D2} (mean speed 54 knots, gusting to 75). The temperature maximum is probably symptomatic of a warm core. Front C_{D1}, which did not pass over Sule Skerry, caused a less dramatic temperature fall - about 1 to 2 deg C. The temperature structure around low D on 14th is illustrated in section 6.

Figure 12 and the pressure gradients on Fig. 10a indicate that throughout low D's lifetime strong winds occurred in a wide arc around its centre, the only region of light winds being northeast of the warm front. Substantial gusts were reported from all stations in northern Scotland which were close to the low track. The following examples show maximum gust (knots), together with report time (UTC) in brackets: North Rona - 84 (13), Sule Skerry - 75 (14), Kirkwall - 60 (16), Wick - 70 (16), Lossiemouth - 48 (16) and Aberdeen - 56 (17).

6: The Structure of Polar Low D on 14th March 1992.

Discussion in section 5(d) emphasised the intensity and developmental nature of low D on 14th March 1992, features which are clearly of interest. This section provides a 'snapshot' of the horizontal and vertical structure of low D around the time of maximum intensity, ie 14UTC on 14th.

Temporal and spatial inhomogeneities in data coverage meant that in order to obtain a satisfactory representation of low D observations from a time-band which spanned 14UTC had to be used. This band essentially ran from 09 to 18UTC on 14th. Such an approach is comparable to using, for example, a research aircraft, whose flight time would typically be 5 to 10 hours. A major input to the investigations was provided by sounding data for 12UTC on 14th, a time at which low D was conveniently located in the middle of the observational region shown on Fig. 1.

Figures 16, 17, 18, 20 and 21 depict horizontal structure, whilst Figs. 19 and 22 depict vertical structure. Considerable input to the cross-section in Fig. 22 was provided by inferences from the other figures.

Figure 16 shows a portion, centred on lows C and D, of the surface analysis for 14th/12UTC in Fig. 10a, together with surface observations for that time. The vast majority of observation parameters are represented. Parameters are displayed as they were reported, except for the pressure from ship 'OW2269' near 61°N 4°W, to which a +4.9hPa correction has been applied. Anomalous data clearly remains, such as the 50 knot wind from ship 'GUMF' near 59°N 2°W. Two other likely errors are noteworthy - pressure is probably 1 to 2 hPa too high at Sule Skerry (section 5(d)(i)), and probably 1hPa too low at Kirkwall (based on similar evidence). The analyst allowed for these errors.

a) Clouds, precipitation and vertical motion

i) Background

Figure 17 shows hourly Meteosat images for 12 to 15UTC on 14th, colour coded in three degree bands according to cloud top temperature (CTT) derived from calibration. Note that Figs. 16 and 17 cover identical regions.

The cloud structure around low D on the 12UTC frame on Fig. 17 is not greatly different from the structure at 0451UTC on Fig. 14. There is still a (ragged-looking) cloud band ahead of the surface warm front position, and a more extensive region of cloud, or cloud head, northeast of the low centre (marked respectively as '{F}' and '{H}' at 13UTC). The coherence of these features and the extent to which they could be distinguished from one another varied erratically (compare frames on fig 17).

The most significant difference between Figs. 14 and 17 is probably the size of the relatively warm (relatively clear) 'core' region around the low centre. At 0451UTC it was about 15km in diameter, but by 12UTC had grown to 50km, and by 15UTC to 140km. The marked expansion of this core region coincided with rapid development of the low, and may thus be a symptom of this development. The radar data in Fig. 12 also shows an absence of convection within the core region (e.g. at 13UTC). This could be explained by subsidence, either above the low centre when low D was at its most intense and/or in an area upwind (in a system-relative sense) just previously.

The solid black contours on the 12UTC frame on Fig. 17 represent 'convective CTT'. Values for this were deduced not from imagery, but from available soundings by performing, on each, a standard 'parcel curve construction', using the surface dewpoint on the sounding and a surface temperature of 8°C (to represent a characteristic sea surface temperature). The temperature extracted from this construction was that attained at the level of zero buoyancy. This level usually coincided with an inversion, such that any overshooting parcels would still have attained a similar temperature. Thus the contoured field should represent the CTT attained over the sea by free convection from the surface layer. Contours were extracted from an initial analysis covering an area about twice as large, encompassing 13 soundings.

The field of 'convective CTT' on Fig. 17 exhibits a large and fairly uniform gradient directed from southwest to northeast. Over the southwest of the domain this gradient is symptomatic of convection (through the cold, unstable arctic air mass) being capped by a sloping large-scale *frontal* inversion, which reaches the surface at the classical warm front in the southwestern corner of the 14th/12UTC frame on Fig. 10a. Above the frontal inversion the airmass is tropical maritime, as indicated earlier. The position of the -36°C contour corresponds to where evidence of this tropical airmass terminates in the radiosonde data. Northeast of this contour the reduction in 'convective CTT' represents solely a deepening of the arctic troposphere.

As the polar low outbreak was confined within the cold air mass, comparison of CTTs on any frame on Fig. 12 with values of 'convective CTT' taken from the 12UTC frame can enable clouds belonging to polar lows C and D and their fronts to be distinguished from clouds in the tropical airmass above. This is clearly a vital first step in interpreting the imagery. For example, any cloud with CTT below -30°C (ie coloured any shade of blue) which exists southwest of the -30°C contour is probably within the tropical airmass. Indeed animated imagery showed such cloud to generally be moving at 65 to 70ms^{-1} (from 310°), a speed much greater than that of clouds with a similar CTT further northeast.

Part of the reason cold front C_{D1}, southwest of low D, appears on the imagery to be a relatively insignificant feature is because it is confined by a frontal inversion whose temperature is around -21°C. Shades of green and blue are generally not seen along C_{D1} because they represent CTTs below this threshold (in the few places they are visible the cause is thin cirrus streaks in the tropical airmass above[1]).

On Fig. 18 data from a variety of sources has been composited together to generate a semi-schematic picture of the distribution of precipitation around low D, and illustrate the relationship between this distribution and features on Figs. 16 and 17. The precipitation distribution is represented by shading in the area where there was radar coverage, and by standard 'station circle' symbols (taken from synoptic reports) near to and beyond the edges of this coverage. Symbols are plotted in 'system-relative' positions where 'system' refers to the *centre* of low D. Account was taken of changes in system velocity (represented on Fig. 9). Small numbers showing reported visibilities are given as a supplementary guide to precipitation intensity. A conversion can be made using equation (1): for example the plotting threshold of 5km corresponds to R = 0.3mmhr^{-1}, or equivalently a snow accumulation rate of about 0.4cmhr^{-1}.

[1] Where *thin* cirrus occurs above a (warmer) low level cloud band that band will be discernible on infra-red imagery, but its *apparent* CTT will be lower than its true CTT. This is because the satellite instrument is summing the radiation emitted by two vertically coincident sources whose temperatures differ, the upper one being insufficiently thick (optically) to obscure the lower.

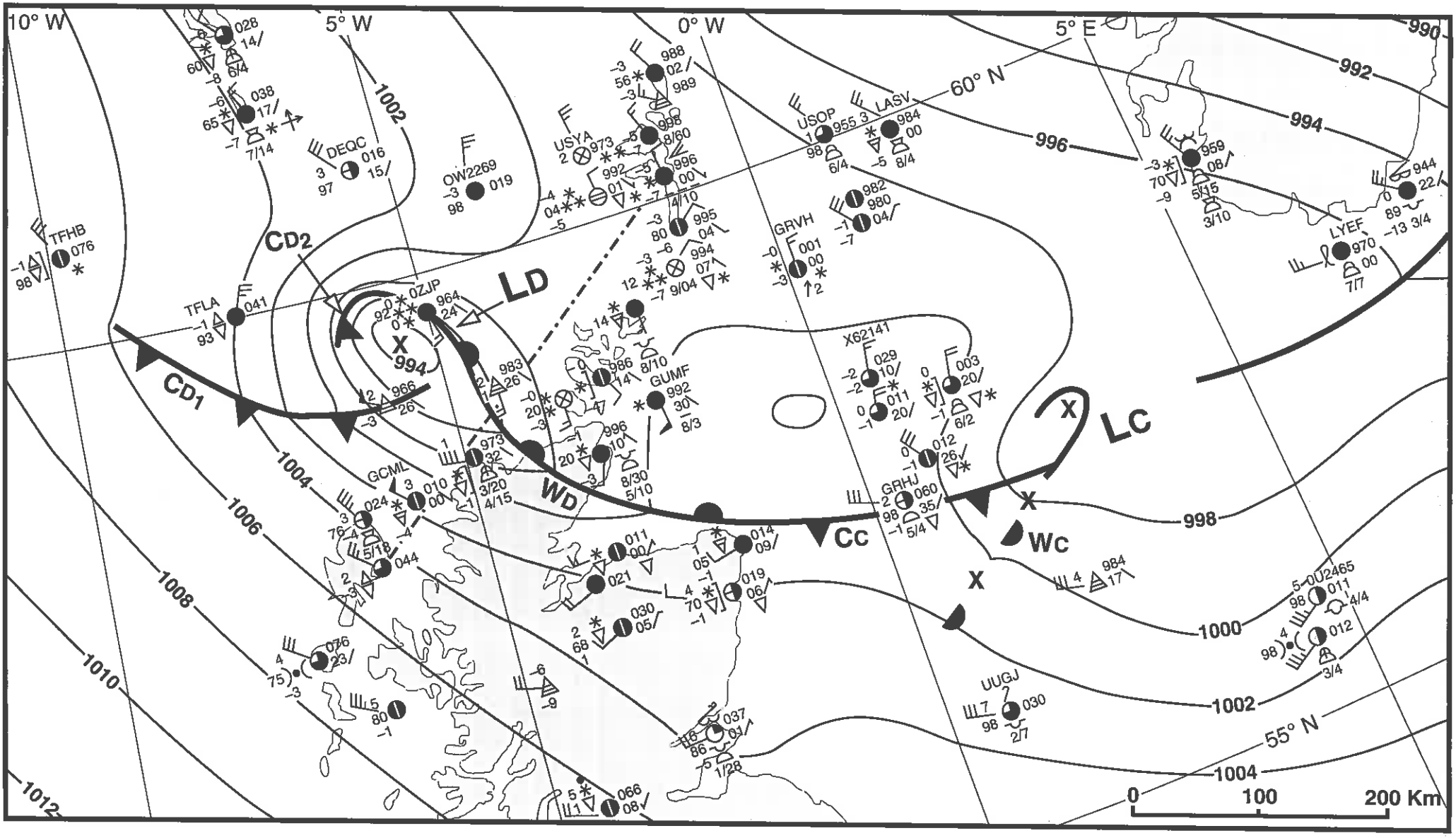

Fig 16: Enlargement of part of surface analysis for 12UTC on 14 March 1992 shown in Fig. 10, with surface observations added (see text). Dash-dot line denotes position of the cross-section in Fig. 22.

93/626-8

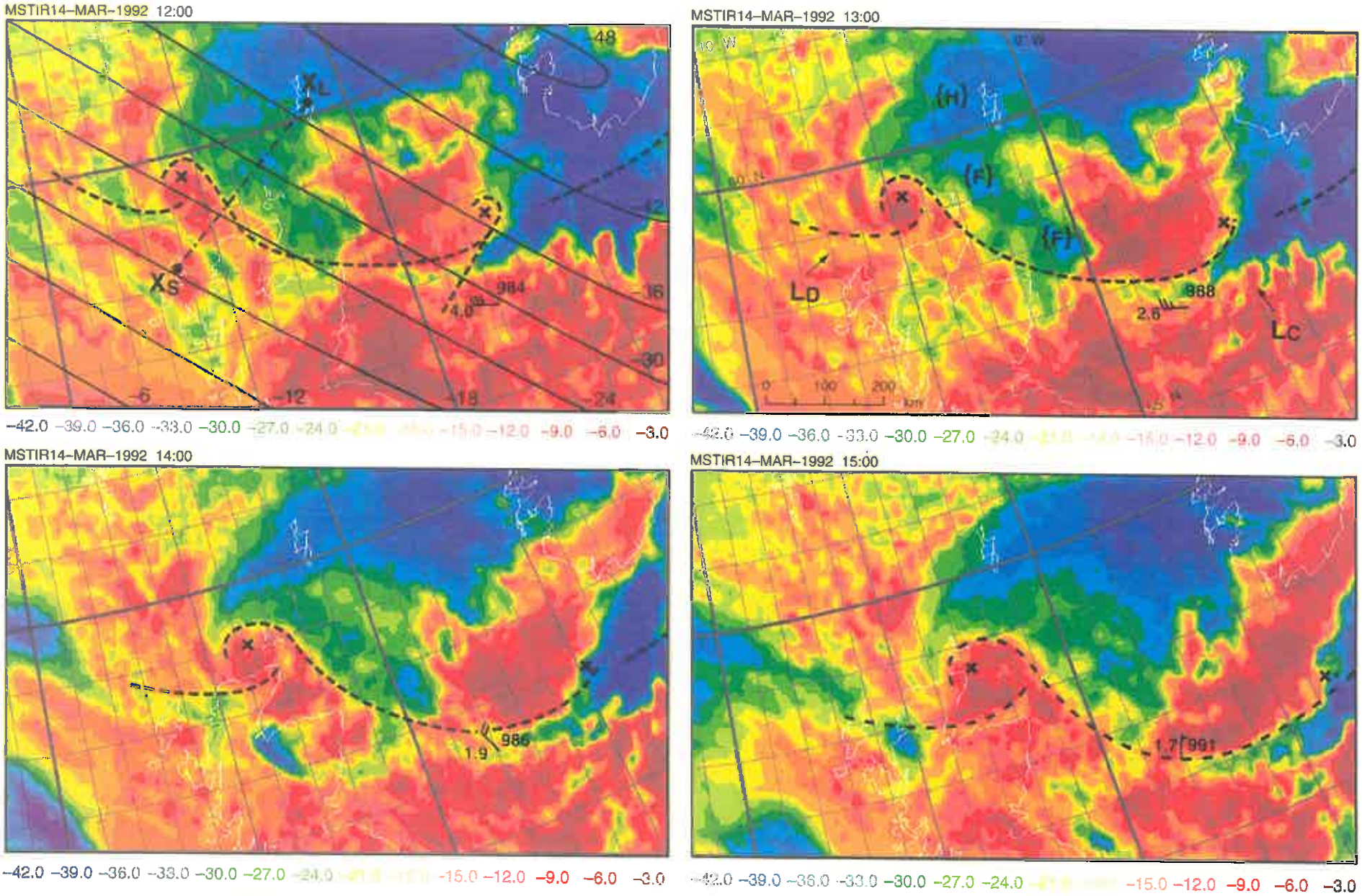

Fig 17: Sequence of hourly Meteosat infra-red images around the time low D attained its minimum central pressure. Colours represent CTT, as given by scales beneath each panel (eg yellow covers range -21 to -18°C). Polar low centres are marked with crosses. Dashed lines show surface positions of (mesoscale) fronts, and of the trough east of low C (see Fig. 10). {F} is the warm front cloud band and {H} the cloud head, as on Fig. 14 (marked only on 13UTC frame). Temperature, pressure and wind reported by one North sea rig are also shown. Dash-dot line on 12UTC panel denotes position of the cross-section in Fig. 22. Contours on 12UTC panel are 'convective CTT' in °C. They essentially represent CTT attained over the sea by free convection from the surface layer (see text). Values correspond to approximate heights (of frontal inversion base / tropopause) as follows: -6°C:780hPa, -12:730, -18:680, -24:630, -30:580, -36:530, -42:480, -48:430.

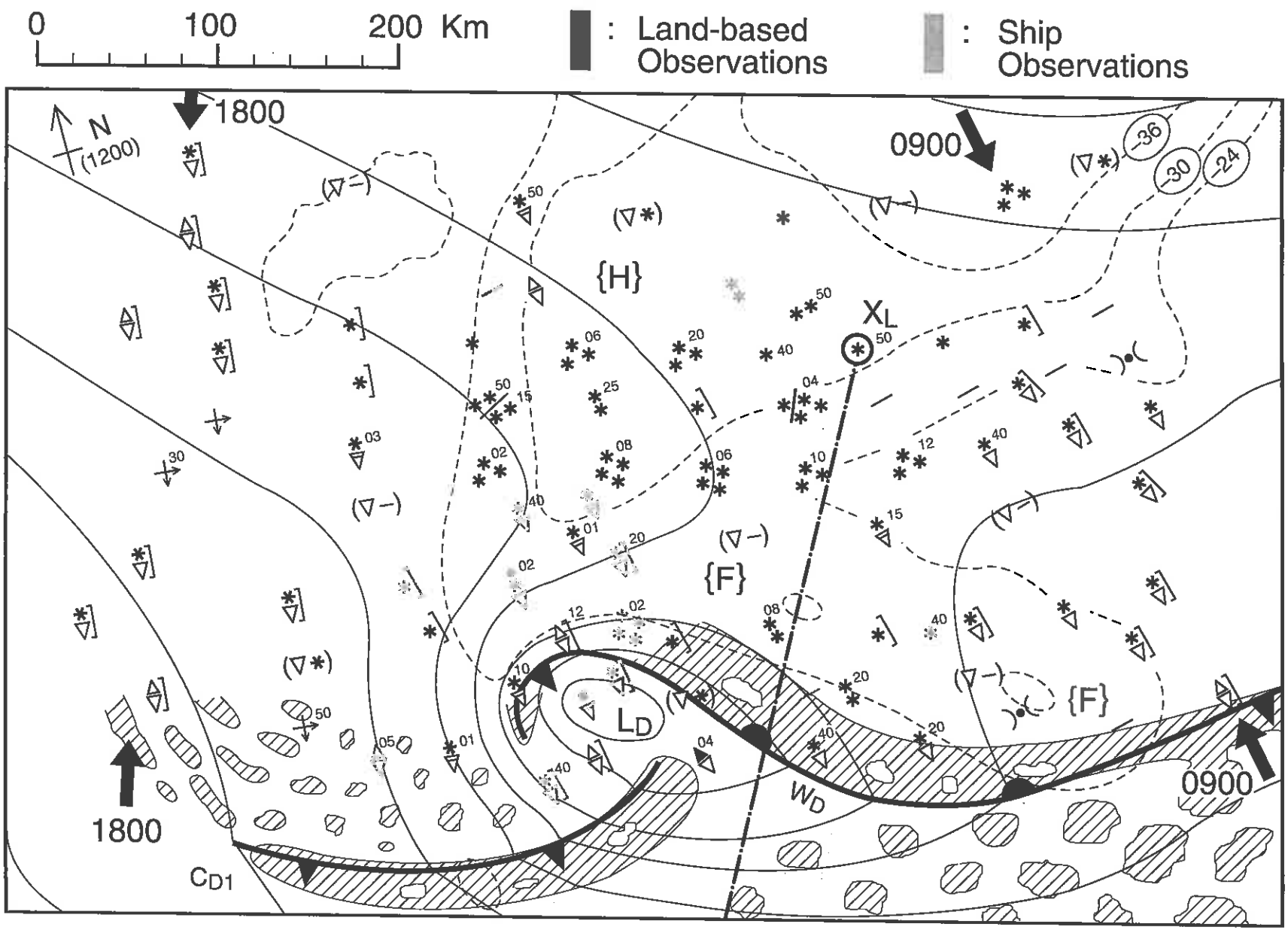

Fig 18: Precipitation distribution around low D. Shaded areas represent precipitation echoes seen on radar data. Symbols depict 'present weather' or 'past weather' observations between 09 and 18UTC on 14th; notation is conventional except that past weather is shown in curved (..) brackets, and 'no reported weather' is denoted by a hyphen. Symbols are centred on their system-relative positions (thus 09UTC observations are mainly on the right, and 18UTC mainly on the left - see large arrows). 'Past weather' is shown only for stations which reported at 3 hour intervals, and is plotted at a position corresponding to 1.5 hours prior to report time. Small figures show visibility in tenths of 1km (not plotted where > 5km). Isobars and fronts are as on Fig. 16. Dashed lines show Meteosat CTT, derived from the 12 and 14UTC frames on Fig. 17; {F} is the warm front cloud band and {H} the cloud head. Dash-dot line denotes location of part of the cross-section in Fig. 22.

As indicated in section 5(d)(v) three reasonably coherent regions of precipitation can be identified in connection with low D: ahead of warm front W_D (and curving back along C_{D2}), underneath the cloud head, and ahead of cold front C_{D1}. Cellular convective precipitation also fell in other areas, notably the warm sector, but had no apparent organisation. In the following three sub-sections (6(a)(ii), (iii) and (iv)) we describe the likely causes of the three coherent precipitation features, and infer some of the probable air parcel trajectories involved. This required synthesis of information from a variety of sources; lists in each sub-section pertain to these sources.

ii) Warm front W_D

It seems that within a 40km-wide band at the surface, which straddled W_D but was essentially on the cold air side, air parcels which had been moving towards the front began to perform near-vertical precipitation-generating ascent, then at some level accelerated towards the east-southeast, and eventually ceased ascending at an altitude of 4 to 5 km, at a location which was 40 to 80km distant, in the across-front direction, from their initial position, the cessation of ascent occurring as they encountered an upper level (classical frontal) inversion and became neutrally buoyant.

Ascent was part of a closed, thermally-direct, 2-dimensional convective circulation, of horizontal wavelength about 80km, in which the descending branch was sufficiently pronounced to inhibit convective development in the otherwise unstable airmass immediately ahead of the warm front precipitation band. This front-parallel 'dry gap' divided precipitation associated with the warm front from that belonging to the cloud head, except in a small area just northeast of the low centre where the two appeared to have merged.

Evidence for the above inferences is given below:

- Radar data showed precipitation extending about 40km ahead of W_D (depicted schematically on Fig. 18), whilst SSM/I data (Fig. 15) showed convective activity extending 20 to 40km ahead.
- Surface winds on either side of W_D (Fig. 16) and the front's rapid northeastward movement (at 30 knots) were such that contributions to the low level front-relative cross-front convergence from the pre-frontal environment were rather greater than those from the post-frontal environment, implying that air parcels from the former would probably have been 'scooped up' as the front approached in preference to those from the latter overrunning.
- The axis of warm front cloud band {F} lay *ahead* of both the surface warm front position (by about 80km) and the warm front precipitation band (by 40 to 80km) (see Fig. 18). This implies that ascending air parcels underwent a lateral forward displacement with respect to the surface front.
- Within frontal cloud band {F} on Fig. 17 CTT was locally less than -30°C (coloured blue). The occurrence of such CTTs in the vicinity of the -30°C convective CTT contour signifies that ascent associated with W_D was probably penetrating into the (classical) frontal inversion. On animated imagery the movement of the coldest cloud tops was much slower than the general northwesterly flow in the tropical airmass above this inversion, suggesting that air parcels had not actually penetrated through it.
- CTT within frontal cloud band {F} corresponded with a height, from soundings, of 4 or 5km, or 600 to 500hPa..
- Out of about 8 reports from beneath the axis of {F}, at only two was precipitation occurring at observation time (Fig. 18).
- Kirkwall, near 59°N, 3°W, provided one such observation (see Figs. 16 and 17). Its full 12UTC cloud report was 7 octas total cloud, comprising 1 octa of stratus at 200m, 3 of stratocumulus at 400m and 7 of stratocumulus at 1km. The fact that an observer looking up from beneath {F} saw less than 8 octas total cloud indicates that {F} was locally quite thin (in a vertical sense). The 12UTC observation was also the first in 61 consecutive hourly observations from Kirkwall to have not included cumulus or cumulonimbus amongst reported cloud types. This implies, given the generally unstable nature of the airmass, that convection from low levels was at this time being greatly inhibited by general descent (descent which may also have thinned the upper level cloud). Within the boundary layer ascent may well have been vigorous, but must have halted abruptly around 1km, the saturated air parcels spreading out there to form a stratocumulus sheet.
- In the area immediately north of the low centre on Fig. 18, where cloud features {F} and {H} merge, there is little evidence of any gap in precipitation.
- Around 23UTC on 14th a radiosonde was released at a location, relative to W_D, very similar to that of the aforementioned Kirkwall observation. The sounding, from Schleswig, is shown in Fig. 19, and its location marked by a black dot on the 15th/00UTC panel on Fig. 10a. The wind veer between 850 and 650hPa implies a thermal wind (in this layer, assuming geostrophic winds) of 310°/40 knots and thermal advection of +29 deg C / day, values which are consistent with a warm front approaching from the southwest. The sounding also shows a moist layer between 510 and 700hPa. This equates to frontal cloud band {F} on Fig. 17, and represents the upper level 'overhang' of cloud

formed by ascent associated with W_D. Conversely there is a very dry layer centred on 800hPa, signifying descent, descent which extrapolation of humidity mixing ratio lines suggests began around 600hPa. The superadiabatic zone seen within the dry layer, between about 740 and 790hPa, has formed as a result of cooling at the top of this dry layer. This cooling was probably due to evaporation of snow falling from the moist layer above (see Clough and Franks, 1991), a layer in which there must have been some general ascent in order for snow to be generated. The sounding thus provided evidence both of the existence of warm front W_D, and of vertically coincident regions of ascent and descent ahead of it.

iii) Cold front C_{D1}

Observational data pertaining to cold front C_{D1} was relatively scarce, principally because of the small scale of the feature. However some deductions could be made.

It seems that in a front-relative frame of reference near-surface air parcels on both sides of C_{D1} were initially converging on the front, but then began to ascend vertically, those in the pre-frontal environment generating an organised 40km-wide band of convective precipitation before decelerating to zero vertical velocity at a height of about 3km, and those in the post-frontal environment generating just localised convective precipitation before reaching zero vertical velocity at a mean height which was rather lower than 3km. Organised compensating descent may well have been occurring in a 50km-wide band beginning at the leading edge of the main precipitation band; this is different to a classical cold front which exhibits descent in the cold air mass.

Evidence for these inferences is given below:

- Radar and (to an extent) SSM/I data on Fig. 15 indicated a 40km-wide band of convective precipitation immediately ahead of C_{D1} (as represented schematically on Fig. 18).
- Cell velocity within the convective region seemed similar to the surface winds there (section 5(d)(iii)), suggesting that any slantwise (front-relative) component to the ascent was small. This is supported by a comparison of Figs. 12 and 17, which showed no major difference between the position (or extent) of the radar echoes and the frontal cloud band (unlike W_D).
- Low level winds (plotted on Fig. 12) and the front's speed of movement were such that contributions from the pre-frontal and post-frontal environments to the low level front-relative cross-front convergence were about equal. As the precipitation was principally on the warm air side, and as the slantwise (front-relative) component to the ascent was small, it follows that converging pre-frontal air must have ascended, for some reason, to a greater altitude than converging post frontal air.
- In the cloud band associated with C_{D1} on Fig. 17 there is a small shortfall between CTT and convective CTT (about 3°C), suggesting that the convective ascent did not penetrate the (large scale) frontal inversion, and was probably less vigorous than that associated with W_D.
- CTT along C_{D1} corresponded with a height, from soundings, of about 3km, or 700hPa.
- Radar data showed fewer echoes immediately ahead of the frontal precipitation band than immediately behind it (see Figs. 12 and 18), hinting that there may have been a band of descent (about 50km wide) *ahead* of C_{D1}'s precipitation band.

iv) The cloud head

The large area of snow found beneath the cloud head was generated not by vertical convection, but by a form of slantwise ascent. The evidence for this inference is listed below:

- In the cloud head region {H} around Shetland on Fig. 17 vertical penetration of ascending air parcels appears to have been limited. For example the zone between the -36 and -42°C convective CTT contours would, if there were vigorous convection, be characterised by clouds coloured in the two darkest shades of blue. This is not seen on any frame.
- On a NOAA visible image for 1445UTC on 14th (not shown) the texture of the cloud head region was considerably more blurred than that of the convective cloud bands associated with Cc and W_D.
- Whilst SSM/I scattering index data in the inset to Fig. 15 showed convective activity on all the fronts, it showed *none at all* in the area occupied by the cloud head (note that the 'snow' axis on the inset represents the system-relative position of the 5 to 6 hours of snow at Fair Isle).
- Convective heating rates *expected* in the cold air mass have been calculated and compared with those 'observed'. This used the empirically-based technique of Blackall found in the Forecasters' reference book (Meteorological Office, 1993), in which an upstream atmospheric sounding is modified on the basis of sea surface temperatures, duration of sea track and expected depth of convection. Twelve hour low-level backward trajectories from 12UTC on 14th, from Stornoway and Lerwick, constructed using the 3-hourly analyses, led to positions which were both within about 200km of Thorshavn, Stornoway's air having initially passed to the north of low D. The 14th/00UTC sounding from Thorshavn was modified according to Blackall, and then compared with the 14th/12UTC

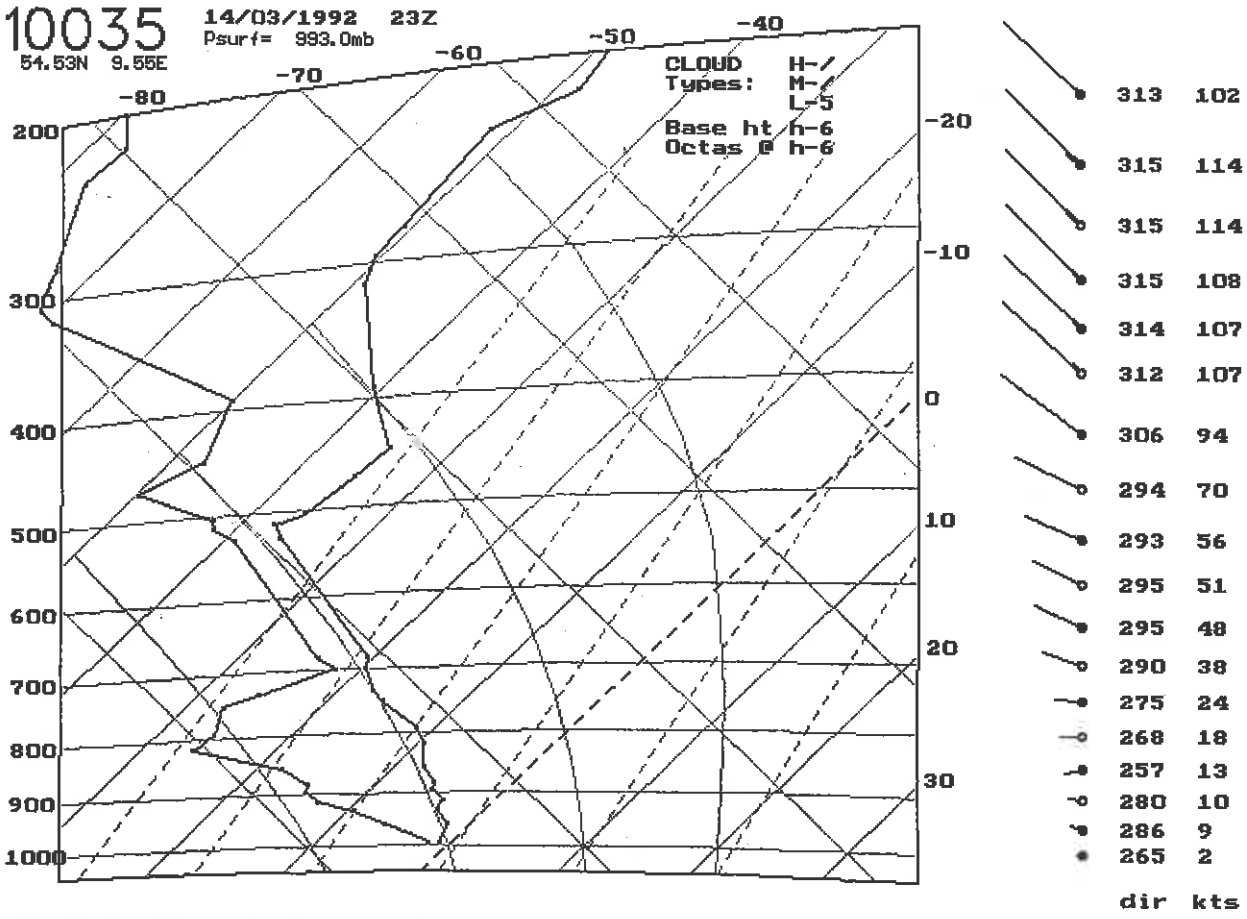

Fig 19: Tephigram for Schleswig timed at 23UTC on 14 March 1992. Wind vectors, interpolated from significant level data, are shown on the right. Pressure levels to which these vectors correspond are given by the tephigram's right hand border. An open circle denotes a pressure which is a multiple of 100hPa. Schleswig's position is shown on the 15th/00UTC frame on Fig. 10a as a black dot.

soundings from the Scottish stations. Convective heating between Thorshavn and Stornoway (as represented on a tephigram by area between the two temperature profiles) showed an excess of between 0 and 30% over that predicted (the 30% uncertainty being due to a change in inversion height) whereas between Thorshavn and Lerwick the heating represented a shortfall of about 50%. These calculations are consistent with there being little convection southeast of and beneath the cloud head, but considerable convection southwest of the mesoscale front Wb/Cc. The difference in heating rates is also frontogenetic, in a broad sense, and would have contributed to the increase in across track baroclinicity noted on Figs. 2 and 7.

- Cloud reports from beneath the main part of the cloud head were analysed closely (for 08 to 15UTC, at Lerwick and Sumburgh, see Fig. 1). The mean number of octas of cumulus was only 0.5, and cumulonimbus was not reported at all. Some low stratus was reported during precipitation. The main cloud type, by far, was dense altostratus (usually 8 octas). This had a base between 6000 and 12000ft, lower values being reported towards the cloud head's northwestern edge. It seems certain that the snow reported from the two stations was being generated within this medium to upper level layered cloud (at Fair Isle, sky was generally obscured from the observer, on account of the intensity of falling snow).

Harrold and Browning (1969) described a large region of uniform slantwise ascent found within a baroclinic polar low. However their observations were over a land mass in winter, where there would have been no high surface temperatures to trigger convection. Over seas at the edges of their observational region convection did occur. What is new in our study is that slantwise ascent was occurring *preferentially* in a region which was rendered exceptionally unstable by the (fixed) temperature of the underlying boundary. This is surprising. Possible reasons are discussed in section (c) below.

In section 5(d)(i) the frontal structure and evolution of low D were likened to those of classical mid-latitude depressions. The cloud head is another similar feature; in the case of mid-latitude depressions its existence is usually a sign of the low having undergone or being about to undergo rapid development. However one aspect of the cloud head region which seems to differ between polar low D and classical lows is the position of the cloud and precipitation in relation to the surface pressure pattern. In mid-latitude lows precipitation remains largely within the surface cyclonic circulation (e.g. Young (1990), Browning and Roberts (1994) and IOP3 in Hewson (1993b)). Yet Fig. 18 shows that the precipitation belonging to head {H} extended well beyond this region; perversely the maximum intensity coincided with the axis of a surface ridge.

b) Thermodynamic structure at the surface

Figures 20 and 21 show the surface distributions around low D of temperature and humidity, humidity being represented by dewpoint depression. The figures were constructed in a similar fashion to Fig. 18 by plotting, in system-relative positions, hourly measurements from stations located close to the track of low D (prior to plotting an offset adjustment was applied to North Rona and Sule Skerry measurements - see Appendix IV).

The analysed temperature field on Fig. 20 seems to represent a broad-scale and fairly uniform across-track temperature gradient onto which a small warm anomaly, about 100 km wide and coinciding with the centre of low D, has been superimposed. The (12UTC) frontal positions are in approximate agreement with the temperature field. Slight inconsistencies would be expected on account of system development and distortion during the 8 hour period to which the plotted values correspond. Temperature gradients appear to be maximised in the vicinity of the bent back warm front (reaching about 6°C per 100km) a feature which is generally observed in standard, intense mid-latitude cyclones (see Neiman and Shapiro (1993) and Browning and Roberts (1994) for examples).

Figure 20 also shows some evidence of a warm core. This is by virtue of the fact that the temperature perturbation observed at Sule Skerry during passage of the low (3 to 3.5°C) was greater than at any other station, a feature which is unaffected by the applied offset adjustments. The small insets show temperature observations in the vicinity of low D at later times on 14th, when it was over the North sea. The high values of 3.5 and 6.9°C registered near the low centre provide some supporting evidence for the warm core.

A composited TOVS 1000-500hPa thickness field based on satellite passes at 1257UTC and 1436UTC on 14th (not shown) showed no evidence of a warm core. The pattern shown was a fairly uniform gradient from southwest to northeast, much as is shown on the 14th/12UTC 1000-500hPa thickness pattern (based on model analysis) on Fig. 2. Possible explanations are that that the warm core was confined to very low levels, that the resolution of the TOVS data (~100km) was insufficient to capture it or that compositing of two passes obscured small scale detail.

On Fig. 21 the areas of high humidity (shaded, for dewpoint depression less than 3°C) generally coincide with areas in which the most persistent precipitation was observed (see Fig. 18). The area

west (left) of cold front C_{D2} also exhibits high humidity, signifying perhaps increased sea surface fluxes in this area. This reasoning is consistent with the strong winds observed here (note the pressure gradients on Fig. 18). The relatively dry region (not shaded) on the top right of the figure is probably associated with descent in a small anticyclone between lows C and D (see Fig. 16). Meanwhile the (right to left) transition from moist to dry in the warm airmass at the foot of the figure coincides approximately with the transition, on Fig. 18, from the showery regime which began in the mesoscale warm sector of low C, to the non-showery regime ahead of the precipitation band of front C_{D1} (noted in section 6(a)(iii)). Note however that there were some showers in relatively dry areas; here the lower humidity probably signified additional drying caused by marked subsidence between convective cells.

c) A Cross Section through low D

i) Background

Figure 22 depicts a semi-schematic cross-section from Stornoway to Lerwick corresponding to 12UTC on 14th. The section cuts the two main precipitation-generating features of low D, namely warm front W_D (cloud marked {F}) and the cloud head (marked {H}). We first discuss the origins of each of the marked features:

- Boundaries of the 'stratosphere/frontal surface' were extracted from an analysis over a larger region, based on a combination of 4 soundings and LAM data. This surface de-lineates the warm tropical maritime airmass (top left) from the cold polar airmass (below).
- Primary and secondary regions of ascending motion were generally marked on the basis of inferences made in section 6(a). However the descending arrow in the top right of the figure was added to signify a warming of the lower stratosphere which had been observed in the vicinity of low D in processed TOVS data. Note that warm anomalies in the lower stratosphere have been observed before in connection with the mature stages of polar lows (Claud *et al* (1992 and 1993)).
- It should be understood that motion was not confined within the plane of the section; the arrows represent the projection of inferred trajectories onto this plane. They are necessarily also schematic because magnitudes of vertical velocities were unknown.
- The regions of solid and broken cloud were also marked using inferences from section 6(a), in combination with surface reports of cloud base, and CTTs from Meteosat imagery. The CTTs were converted to approximate cloud top pressure using the Stornoway and Lerwick soundings in conjunction with the marked position of the 'stratosphere/frontal surface'. As this surface was essentially isothermal it was not possible to deduce precisely, from CTT, the positions of cloud tops which fell within it. There is also some uncertainty in the height of cloud base in regions of moderate or heavy snow, because surface reports in such regions generally showed 'sky obscured' (by the falling snow).
- Schematic precipitation symbols are based on Fig. 18.
- Contoured fields came from a 2-dimensional objective analysis of data on the sides and base of the domain shown (see Appendix V).
- The lack of input data at high levels in the centre of the cross-section renders the objectively analysed fields there as unreliable. For this reason contour thresholds were selected such that plotting was mainly confined to low levels.
- The quantity 'cross-front divergence' was derived from components of the wind perpendicular to the orientation of the *surface* front, and as such has little meaning at high levels. Contours of this variable have only been shown below 700hPa.
- Contours of absolute momentum, $M = v + fx$, were shown on Fig. 22 mainly for the purposes of assessing, qualitatively, the instability to slantwise convection (ie conditional symmetric instability (CSI)) of the atmosphere in the vicinity of the polar low. The x-axis points towards 060° (ie perpendicular to the tropospheric thermal wind, which was deduced on the basis of Fig. 2 to be oriented towards 130°).

Theories of CSI (see Bennetts and Hoskins (1979) and Emanuel (1983a,b)) usually assume 2-dimensional geostrophic motion, whereby vertical wind shears (or thermal winds) within the 3-dimensional domain under consideration are everywhere unidirectional. If Fig. 22 is to be used for assessment of CSI it is helpful to first check the extent to which this assumption has been satisfied in our case. Within the plane of the cross section winds (plotted around the edge) have one dominant direction (northwesterly), and show a general increase in speed with height. As such they are reasonably consistent with the requirement of unidirectional shear. Recall that in section 5(d)(ii) the lower tropospheric thermal wind in the region immediately ahead of warm front W_D was also deduced to be northwesterly. In the y (long-shear) direction the unidirectionality should extend across a distance $L >> U_0/f$ (Emanuel (1983b)), where U_0 is a typical velocity of the high level jet. In our case

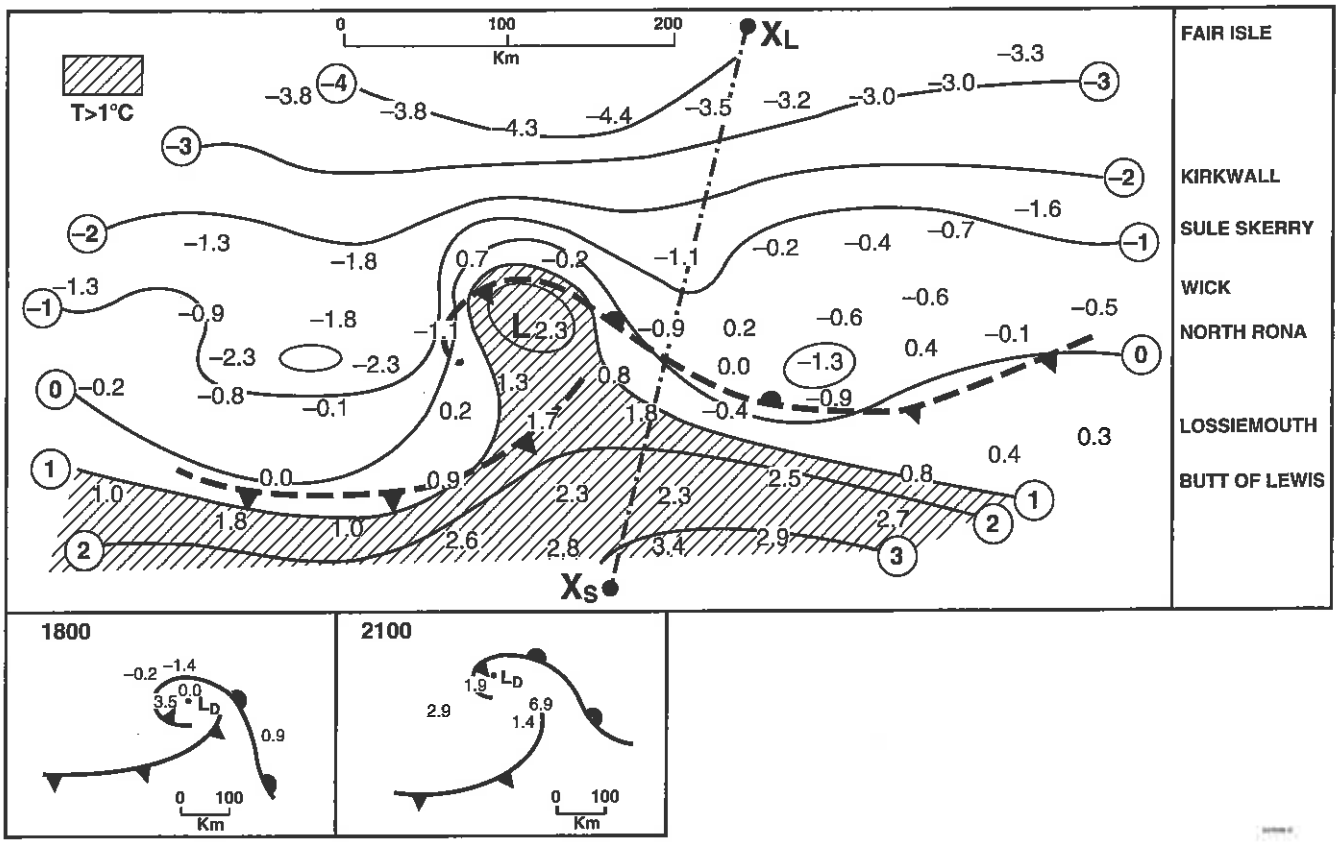

Fig 20: Large panel: Surface temperature distribution around low D. Values are hourly temperature observations from stations named on the right, for 09 to 17UTC on 14 March 1992, plotted in system-relative positions. Offset adjustments have been applied to observations from Sule Skerry and North Rona. Contours are hand-drawn; values greater than 3°C are shaded. Fronts are as on Fig. 16. Dash-dot line shows position of the cross-section in Fig. 22. Also see text. **Small panels:** Temperature observations in the vicinity of low D at 18 and 21UTC on 14 March 1992.

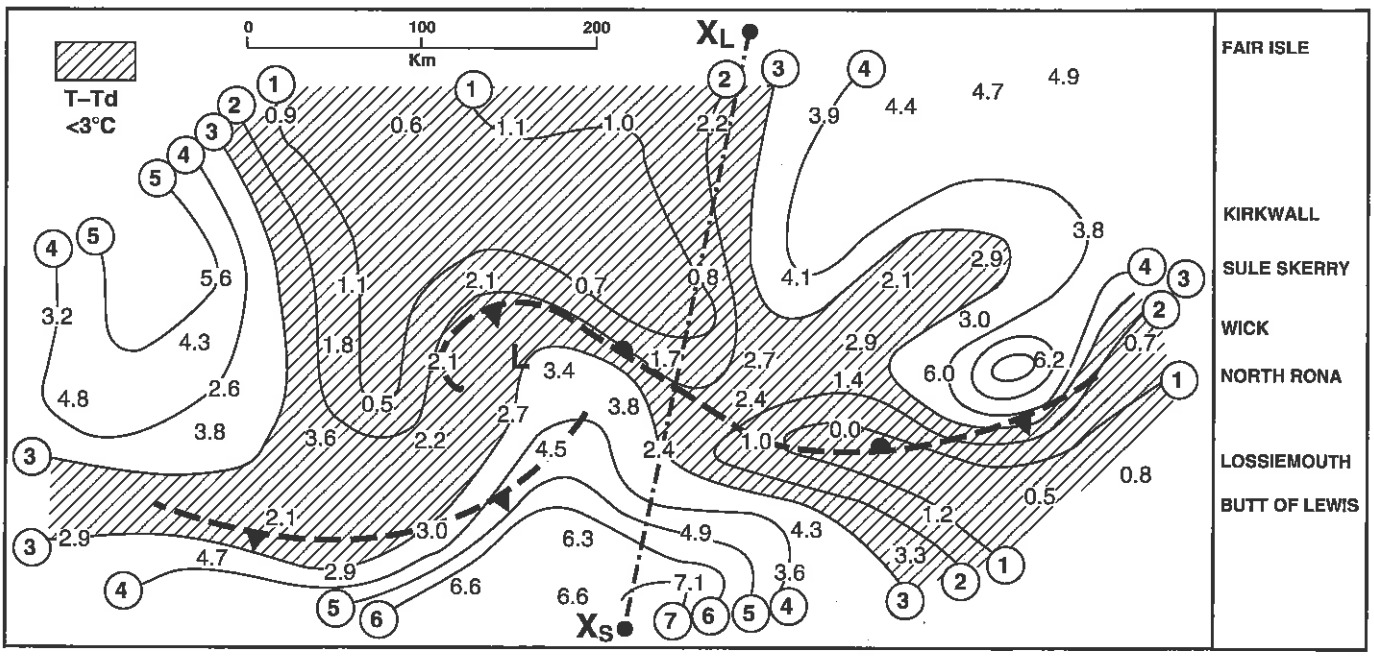

Fig 21: Humidity distribution around low D, shown as dewpoint depression. Values correspond to hourly observations from stations named on the right, for 09 to 17UTC on 14 March 1992, plotted in system-relative positions. Offset adjustments have been applied to observations from Sule Skerry and North Rona. Contours are hand-drawn; values less than 3°C are shaded (ie high humidity). Fronts are as on Fig. 16. Dash-dot line shows position of the cross-section in Fig. 22. Also see text.

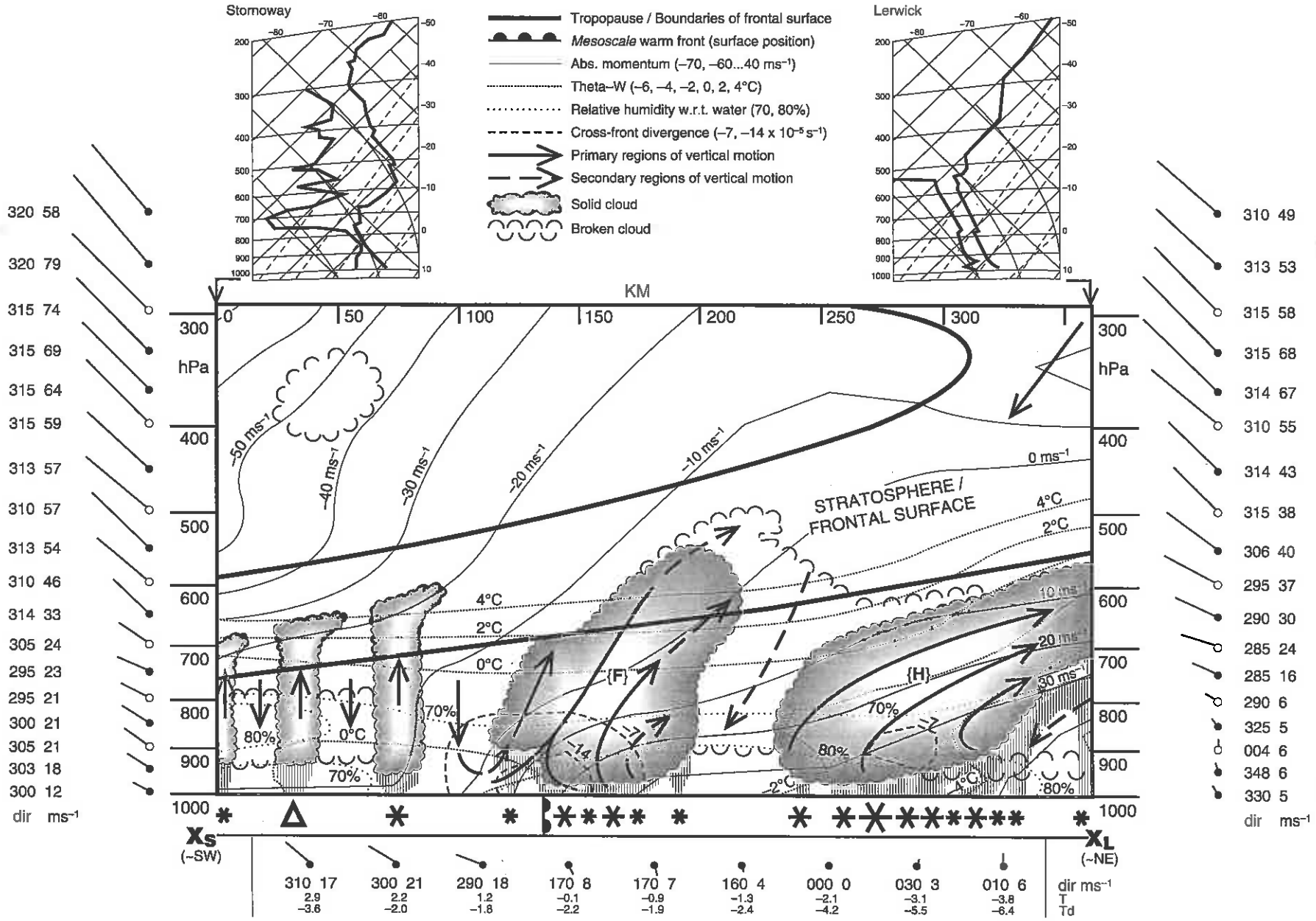

Fig 22: A semi-schematic cross-section (central panel) through cloud features associated with low D, for 12UTC, 14 March 1992. Section runs from Stornoway (left, X_S) to Lerwick (right, X_L). Its position is marked on Figs. 2, 12, 16, 17, 18, 20 and 21. Key (centre top) indicates the meaning of the marked features; their origins are described in the text. Radiosonde data for Stornoway and Lerwick (for 14th/12UTC) is shown at top of figure (tephigrams) and at the sides (winds). Wind vectors correspond to adjacent pressure levels on the section (open circles denote correspondance to pressure levels which are multiples of 100hPa). Schematic symbols immediately beneath the section indicate precipitation location, type and intensity (larger = heavier), and surface position of (mesoscale) warm front WD. Beneath this are shown surface winds, temperatures and dewpoints.

the 'high level' jet, taken at the top of the arctic troposphere, is about 40ms^{-1}, giving the requirement L >> 300km. Other radiosonde data outside the plane of the section (notably from Thorshavn, about 300km away) suggested that there was unidirectional shear across such distances. This deduction is supported by the straightness of the thickness lines on Fig. 2. Thus the situation we are considering seems to be one in which the assessment of CSI is potentially quite meaningful.

It could be argued that the position of momentum surfaces within the domain is really unknown, on account of the lack of sounding data. However values of absolute momentum *are* known along the sides and the base, implying that if matching values can be found on these boundaries the two respective locations must be connected by a single contour. In addition the general pattern of momentum lines shown beneath the stratosphere/frontal inversion (in particular the variations in slope) is very similar to that represented on 'real' cross-sections extracted in equivalent system-relative locations from a successful numerical model forecast of another intense low with a cloud head (Shutts, 1990) suggesting that our pattern is quite a plausible one.

To deduce air mass trajectories authors often consider that motion follows surfaces of constant 'ambient' theta-W, as portrayed in 3-dimensional analyses of observational data, an inherent assumption being that vertical velocities can be derived from the projection of horizontal winds onto these ambient surfaces (as in Harrold and Browning (1969) and Browning and Roberts (1994); see also Locatelli et al (1994)). This method is most appropriate for diagnosing large scale ascent in stable regimes. It would be less appropriate to use for our case however for two (related) reasons; low D developed in an unstable environment, and ascent in this environment consisted mostly of small scale convection.

In discussing trajectories below for our case we appeal instead to *parcel* theory, in which ascending air parcels attain their vertical velocities *in situ*, as available potential energy, provided by a combination of convective and inertial instability, is converted to kinetic energy. Such air parcels should conserve both their own theta-W and absolute momentum as they ascend. However this does not necessarily mean that the path of ascent will follow either ambient theta-W or ambient momentum surfaces of the surrounding environment; a compromise is more likely. Indeed in a convectively mixed environment the few ambient theta-W surfaces portrayed may well not follow a coherent, traceable pattern, and it may therefore be more convenient to assume that trajectories approximately follow ambient momentum surfaces. This assumption has generally been employed in the discussion below.

ii) Structure

The cross-section in Fig. 22 shows 4 separate regions of 'significant' cloud; a patch of cirrus in the tropical maritime airmass (top left), vertical convective cells in the mesoscale warm sector (lower left), a forward-sloping region of frontal cloud (marked {F}), and a second region of forward-sloping cloud representing the cloud head (marked {H}).

In the area of vertical convection the momentum is 'well-mixed' with contours, such as -10ms^{-1}, being essentially vertical (the horizontal segment of the -10ms^{-1} contour probably reflects near-surface frictional effects). Here air parcels have little choice but to ascend vertically, triggered by heating from the warm sea surface below. The Stornoway sounding is within this regime. The resemblance of the lower part of its tephigram (below 780hPa) to a standard parcel curve construction is a sign of vertical convection; similarly the narrow layer of higher humidity within the frontal inversion around 610hPa may represent lateral advection from the anvil region of a cumulonimbus cloud which has penetrated this inversion. Cloud bases in this region are higher, generally, than in the cloud systems further east on account of lower surface humidity (note the 70% relative humidity contour).

The momentum surfaces within frontal cloud band {F} are less vertical, consistent with there being some slantwise component to the motion, at least at upper levels, but still a substantial element of vertical convection. The front appears to have a general slope of about 1 in 15 (calculated from the surface position to the height of the coldest cloud tops). This is an order of magnitude less than that of a typical mid-latitude warm front, such as the one associated with the frontal surface marked on the section. This difference is presumably due to a large instability to underlying sea surface temperatures on both sides of the (mesoscale) front. Cloud bases to the southwest (left) of the surface front are higher than those to the northeast as a result of the ascending air to the southwest having relatively dry origins. These origins comprise a region of descent immediately behind the front and/or the boundary layer in the area of vertical convection.

Within the cloud head region {H} the momentum lines have a relatively shallow slope, of about 1 in 80, which might suggest, at first sight, relatively small vertical velocities, and hence relatively little precipitation. However part, if not most, of this cloud head region appears to be unstable to slantwise convection. Consider, for example, the 20 and 30ms^{-1} absolute momentum contours. The values of theta-W at their western ends are respectively about 0 and -1°C, and at their eastern ends about -3

and -4°C. The *reduction* implies CSI. This must be present at least somewhere along each contour, irrespective of the precise behaviour of the fields of either theta-W or absolute momentum within the plane of the cross-section. Release of such instability is partly constrained by the humidity. However available cloud, precipitation and humidity observations suggested that the air was nearly or completely saturated, at least with respect to ice. Thus in the absence of any evidence of vertical convection the realisation of CSI appears to offer a plausible explanation for the heavy snow observed beneath the cloud head. In a region of CSI trajectories followed by ascending air parcels are difficult to evaluate, although it is likely that there will be a compromise between conserving angular momentum and conserving theta-W. Simplified theory suggests that where theta-W surfaces are almost vertical and momentum surfaces almost horizontal, as seems to be the case in at least the lower part of the cloud head, any ascending parcels will *begin* to move at 45° to the vertical, then subsequently acquire a more horizontal trajectory (Emanuel (1983a)). This is consistent with the trajectories drawn. It may well be that initial near-vertical ascent generated most of the observed snow.

It has been suggested (e.g. Shutts, 1990) that slantwise convection in a cloud head region can be a precursor of and contributing factor for the rapid development of mid-latitude depressions, such as the 1987 October storm, which indeed displayed a very prominent cloud head during its period of most rapid development. Perhaps then rapidly developing polar lows, such as our low D, can have similar characteristics.

Shutts emphasised one feature on high resolution satellite imagery which could be indicative of the presence of slantwise convection, namely narrow striations (in the cloud head) which have an orientation perpendicular to the thermal wind (see also Norris and Young, 1991). Striations such as this can be seen at a time prior to the rapid development of low D, on Fig. 14, in the region immediately west of the Faeroes (oriented southwest to northeast). Similar striations are apparent on other NOAA images (not shown), for 0810 and 1445UTC. On the 1445UTC image they are particularly evident directly above Fair Isle, which reported the heaviest, most persistent snow.

Some caveats should be added here. It was possible to detect what appeared to be 'striations' in a number of places on NOAA imagery during the polar low outbreak, and with a variety of orientations; implying either that slantwise convection occurred quite widely, or that striations alone are not a good indicator. Secondly the hypothesis that slantwise convection can contribute to rapid development relies, at least in Shutts (1990), on vortex spin-up being aided by slantwise convective mass transfer. In our case the projected two-dimensional trajectories depicted on Fig. 22 suggest that displacements through the cloud head did not involve extraction of mass from a region near to the low centre (the surface (mesoscale) warm front is closest to this centre). The trajectories do not connect with this region because there is a gap between precipitating regions {F} and {H}. However closer in to the low centre there was apparently no gap, suggesting that slantwise convective mass transfer there probably *could* have contributed to vortex spin-up.

7: Summary and concluding discussion

Between 12th and 14th March 1992 a region of exceptionally cold arctic air advected southeastwards across Iceland, northern Scotland and on into mainland Europe. Four polar lows (A, B, C and D) were identified during the period, occurring generally on the southwestern flank of the axis of coldest air. Detailed analysis of routine synoptic observations, routine soundings, radar data from a new site in Scotland, and raw and processed satellite imagery enabled the tracks, the mesoscale structure and particularly the evolution of these polar lows to be described in detail. In this concluding section we summarise the main features of the polar lows, and briefly discuss why their mesoscale fronts might have the characteristics listed in section 3b.

The polar lows developed and evolved *beneath* a sloping, large-scale frontal inversion associated with a classical warm front which was slowly advancing from the southwest. There was no evidence of any interaction with the large-scale surface front.

The structures and evolutions of the four polar lows exhibited great variety. One polar low (A) was essentially convective, the other three baroclinic. Development of the weakest low (B) was forced by an upper level trough, yet the most intense low (D) developed in the absence of perceptible upper level forcing. Lifetimes ranged from 15 hours (B) to over 2 days (D). Two lows decayed rapidly on encountering land (A, B), one re-intensified over land (D), and the other decayed over sea (C). Speeds of movement of the low centres (at given times) ranged from about 9 to 24ms^{-1}. No general connection between development and speed of movement was apparent, although there was acceleration during periods of decay. Relative vorticity at the centre of the most intense low (D), reached about 5f. The intensity of low D was comparable with that of other unusually severe Atlantic storms, although its horizontal dimensions were considerably smaller.

Wind speeds around the lows were highly variable although the strongest winds always occurred on the southwestern flank. This was consistent with the background synoptic scale flow, which was northwesterly. Highest gusts were associated with lows A and D, reaching over 70 knots. In the case of A this maximum could be attributed to the effect of adding a small perturbation to a strong background flow (see Aakjaer, 1992), whereas for D the background flow was weaker (by about 50%) and the low itself particularly intense.

Coherent, small scale, front-like features were identified around all four lows, features which could be tracked in time (in one case for 36 hours). These features were termed 'mesoscale' fronts. Their horizontal dimensions were much smaller than those of classical fronts, the size ratio being about 0.2. Around lows C and D the (mesoscale) frontal configurations were similar in appearance to those typical of much larger baroclinic lows. In addition the evolution around low D of its (mesoscale) fronts resembled that seen in the Shapiro/Keyser (1990) conceptual model of a rapidly developing cyclone.

The 2 mesoscale warm fronts identified were analogous to classical warm fronts in that precipitation occurred ahead of the surface front. One estimate gave a frontal slope of 1 in 15, which is an order of magnitude greater (steeper) than the slope of a classical warm front.

Out of 4 mesoscale cold fronts identified 3 had precipitation bands which were essentially ahead of the surface front. In these cases the frontal surface must have been almost vertical. Although this picture differs from the classical *kata* cold front (which has rearward sloping ascent and precipitation concentrated in the cold air) it does resemble a classical *ana* cold front, and also the cold front depicted in the Shapiro/Keyser (1990) conceptual cyclone model (see also Neiman et al (1993)).

Large areas of cloud were identified northeast of lows C and D. The first was highly convective and was linked to marked isobaric troughing at the surface, whilst the second was not convective and had no signature in the surface pressure pattern. This second feature was labelled a 'cloud head', by analogy with intense classical mid-latitude depressions. Further analysis showed evidence of instability to slantwise convection in this cloud head region, suggesting that slantwise convection could have been both the source of the observed precipitation, and a contributor to the marked intensification of the low.

Out of features which have hitherto been associated with classical mid-latitude depressions, the following were identified, in a smaller form, amongst the polar lows investigated in this study: (mesoscale) warm and cold fronts (A, B, C and D), warm sectors (C and D), an 'instant occlusion' (C, some evidence), a wave train (C to D), a bent back warm front (D), strongest temperature gradients along the bent back warm front (D), a 'T-bone' structure (D), frontal fracture (D, some evidence), warm seclusion (D, some evidence), a cloud head (D) and 'striations' within that cloud head (D). These features were more prevalent when the low level baroclinicity was enhanced (this was greatest across D, about 7°C over 400km).

Characteristic	Feature		
	(i) Mesoscale fronts	(ii) Convection in mesoscale warm sectors	(iii) Surface trough + (iv) cloud head
Width of band (km)	30-80	-	100-150
Duration of ppn. (hrs)	0.5-2.0	(6) (intermittent)	3-6
Total (D_R) (mm)	0.4-2.0	(1.5)	~10
Total (Ds) (cm)	0.5-2.5	(1.9)	~10-15
Mean rate (rain) ($mmhr^{-1}$)	0.9	0.25	~2.2
Mean rate (snow accumulation) ($cmhr^{-1}$)	1.1	0.3	~2.8
Max. rate (rain) ($mmhr^{-1}$)	2.0-4.0	3.0	~4
Max. rate (snow accumulation) ($cmhr^{-1}$)	2.5-5.0	4.0	~5

Table 2: *General* precipitation characteristics associated with specific features of polar lows B, C and D. Values given refer to fixed locations near the coasts of northern Scotland, and assume there has been no decay of precipitation over land - precipitation from most features generally disappeared completely after a 150km passage across land. Areas of convection in the mesoscale warm sector(s) were wedge shaped, and thus had no characteristic width or duration; bracketed values assume intermittent convective precipitation lasting 6 hours.

Precipitation associated with the polar lows was predominantly snow. Around lows B, C and D four distinct precipitating regions were identified: (i) convective bands associated with the mesoscale

fronts, (ii) scattered convective cells within the mesoscale warm sector, (iii) deep convection along the surface trough line (northeast of C) and (iv) non-convective precipitation in the 'cloud head' (northeast of D). Table 2 summarises the *general* precipitation characteristics in these regions. Types (iii) and (iv) are grouped together as their (quoted) characteristics were similar.

It is clear from the table that the mesoscale fronts were not especially active in terms of precipitation. In comparison with the trough northeast of C or the cloud head northeast of D they produced less wide bands of precipitation, shorter durations, smaller totals and lower intensities. In the case of totals the difference was about one order of magnitude. Thus the heaviest precipitation clearly occurred to the left of the polar low tracks (as has been found in other cases, e.g. Lyall (1969) and Aakjaer (1992)).

Precipitation associated with the mesoscale fronts was predominantly convective. This is consistent with the airmasses on either side of these fronts having been unstable to (observed) sea surface temperatures. The fact that the convection was organised into front-parallel bands (one per front) suggests that frictionally-induced low-level convergence, coinciding with the fronts' surface pressure troughs, provided a sufficient trigger for organised release of the instability. Over land, whilst there may still have been convergence, the ultimate energy source for the convection, a high surface temperature, was lost. It is thus not surprising that precipitation died out fairly readily over land (within about 150km). The lack of a moisture source probably also contributed to the decay.

In simple Ekman layer theory low level convergence increases with both ζ_g and the angle (α) between surface winds and isobars. As stability decreases α decreases also. Our very unstable 'mesoscale front regime' (small α) can thus be compared to a relatively stable 'classical front regime' (large α). To achieve a set amount of low level convergence our regime would require a relatively large value of ζ_g. This may partly explain why the mesoscale fronts had marked vorticity signatures (compared to classical fronts) yet exhibited precipitation rates which were not particularly high (column (i) in Table 2).

The absence of marked thermal signatures and the steep frontal slopes can probably also be attributed to the very unstable nature of the airmasses involved. It is not possible to maintain either sharp temperature gradients or thin wedges of colder air at the surface when there are very large upward heat fluxes from that surface. These fluxes are larger where the air is colder, and thus act to to smooth out any temperature discontinuities. The only way to counteract such a frontolytic effect would seem to be by having stronger winds on the warm side of the temperature discontinuity. Perhaps then a key feature of the (mesoscale) fronts which helped them maintain their identities was the existence of stronger winds in the warmer airmass.

Acknowledgements

Adrian Todkill provided synoptic data for re-analysis, and John Williams the radar data. Clare Davitt generated objectively analysed fields for the cross-section whilst Gill Dale drafted most of the figures. The work also benefited from discussions with Craig Bishop, Keith Browning, Sid Clough, Alan Thorpe, John Thomason and Ross Reynolds.

APPENDIX I.

Geostrophic relative vorticity:

Values of geostrophic relative vorticity (ζ_g) were derived manually from hand drawn surface pressure analyses using the standard method, given in Gyakum et al (1992):

$$\zeta_g = 4 (P - P_c) / \rho f \Delta^2$$

where P_c is the pressure at the centre of a regular four point cross, P is the mean of the pressures at the four points, ρ is the air density, f is the coriolis parameter, and Δ is the distance from cross centre to cross point. The following 'constant' values were used: $\rho = 1.28$ kg m^{-3}, $f = 1.259 \times 10^{-4}$ s^{-1} (for 60°N), and $\Delta = 100$ km.

APPENDIX II.

Representativeness of temperature measurements:

In regimes where the atmosphere is rendered very unstable by heat fluxes from the underlying sea surface (as in our polar low outbreak), screen-level temperatures at a given location become very prone to fluctuations caused by factors other than the passage of a front. Temperatures will drop during precipitation. They will also drop if a subtle change of wind direction results in an increased passage across land of the surface air. A change of land track from zero to a few km can result in a temperature fall of as much as a few deg C, for example. Night time radiative cooling over snow covered surfaces can also produce dramatic temperature falls. These factors generally affect the temperature of the lowest few tens of metres of the atmosphere, or surface layer. Airmass characteristics would be much better signified by measurements from the top of this layer. Unfortunately screen-level measurements (such as were available for this study) are not taken at such heights. For these reasons care must be taken during analysis to not attach too much importance to screen temperature fluctuations, nor to expect there to necessarily be an obvious discontinuity in screen temperatures along any fronts.

APPENDIX III.

On the use of SSM/I wind speeds:

Fields of SSM/I-derived surface wind speeds are potentially a very useful aid for analysing surface charts over sea areas. Although there is not the directional element available with ERS-1 data (Bell, 1994) the temporal and spatial coverage at high latitudes is much better, and careful scrutiny of the analysed speeds can allow deductions to be made about directions, as indicated in (3) below.

If the surface winds can be assumed to be in geostrophic balance (not unreasonable given that operational models use such an assumption to good effect (Bell, 1994)), then it follows that:

(1) Isobaric spacing should be inversely proportional to wind speed (allowing for variations in f)

(2) Near-straight discontinuities in wind speed will usually indicate a surface trough (as on Fig. A1), and thus, often, a front.

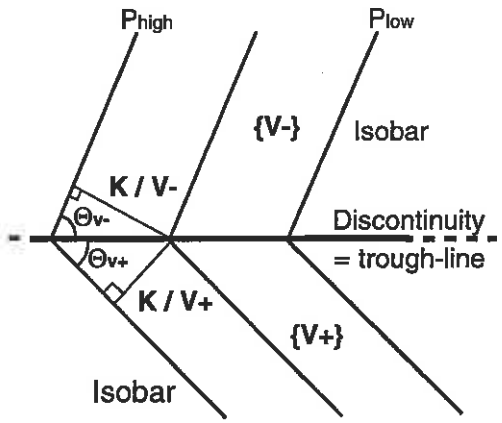

Fig A1: The isobaric pattern implied by a near-straight discontinuity in wind speed on an SSM/I image. The wind speeds are V- and V+ and are assumed geostrophic; V+ is the larger. A trough line coincides with the wind speed discontinuity; isobars are assumed to be straight beyond this line. Isobaric spacing is inversely proportional to geostrophic wind; if the constant of proportionality is 'K' the isobaric spacing is (K / V-) where wind speed is V-, and (K / V+) where wind speed is V+.

(3) If isobars in the vicinity of a trough-line identified by (2) can be assumed to bend only along that trough-line then it follows, from the two triangles constructed on Fig. A1, that

$$\sin(\Theta_{v+}) / (K / V_+) = \sin(\Theta_{v-}) / (K / V_-)$$

ie $\sin(\Theta_{V+}) / \sin(\Theta_{V-}) = V- / V+$ (A1)

where $V+$ and $V-$ are the wind speeds (respectively strong and light) identified on either side of the trough-line, and Θ_{V+} and Θ_{V-} are the angles between trough-line and isobars on these (respective) sides.

Then:

a) the angle between isobars and trough-line in the zone of stronger winds (Θ_{V+},), is constrained to be less than a particular value, which we call $\Theta_{V+(max)}$, by the fact that ($\sin(\Theta_{V-})$) has to be less than or equal to 1. This value is given by:

$$\Theta_{V+(max)} = \sin^{-1}(V- / V+) \quad (A2)$$

where $\Theta_{V+(max)} < 90^{\circ}$.

b) if there are sufficient surface observations to deduce the angle between isobars and trough-line in *either* the strong wind zone (Θ_{V+}) or the light wind zone (Θ_{V-}), then the corresponding angle in the other zone can be deduced from Eq. (A1) above.

In Eq. (A2) relatively small differences in wind speed put quite a large constraint on Θ_{V+}, rendering the equation more useful than might at first seem the case. For example a 30% difference gives $\Theta_{V+(max)}$ to be 45°. However there is a special case in which a trough-line will not show up as a wind speed discontinuity. Putting $V+ = V-$ in Eq. (A1) does not imply that both Θ values are 90° (as would be the case were there no trough, see Fig. A1), but just that their sines are the same.

APPENDIX IV.

Offset Temperature/Dewpoint Adjustments

Two of the stations used to construct Figs. 20 and 21, North Rona and Sule Skerry, were located on tiny isolated islands (less than about 1km across). It was felt that this could make their temperature and dewpoint measurements incompatible with those from nearby stations, where the land track was generally larger, for reasons given in Appendix II. Specifically, the measurements were expected to be too high (relatively). For this reason offset adjustments were applied to the measurements from the two stations.

In order to derive the offset adjustments we first defined an 'across-track' co-ordinate. This co-ordinate was perpendicular to low D's track, and had a positive direction to the left of this track. The offsets were then calculated from the following equation:

$$\Delta T_S = T_1 + (X_{1S} / X_{12}) (T_2 - T_1) \quad (2)$$

where subscripts 'S', '1' and '2' refer respectively to the station whose measurements are being corrected, the closest station in the 'negative across-track' direction, and the closest station in the 'positive across-track' direction; ΔT is the temperature offset, T is the mean temperature between 09 and 17UTC, and X is 'across-track' distance (ie co-ordinate of the second subscripted location minus co-ordinate of the first). Stations '1' and '2' were selected only from those named on Figs. 20 and 21. Dewpoints were corrected in the same way as temperature.

Offsets applied to the Sule Skerry temperature and dewpoint observations were about -3°C. At North Rona they were almost negligible, probably because the relatively high altitude of the station (108m) was compensating for the smallness of the island on which it was located.

APPENDIX V.

Objective Analysis

The objective analysis procedure is summarised in Hewson (1993b) and described fully in Pedder (1993). The input dataset comprised values of 5 basic variables P, U, V, T and relative humidity (derived from T and T_d) at various datapoints on the borders of the cross-section domain shown (Fig. 22, all input data is depicted). These datapoints were spaced at intervals of 50hPa or less on the vertical edges of the domain (extracted from the 12UTC Lerwick and Stornoway sound-

ings) and at 36km intervals along the base (from surface measurements on Figs. 16, 20 and 21). The objective analysis involved initially analysing the observed variables onto a regular x-z grid (with respective horizontal and vertical grid spacings of 36km and 0.4km (~40hPa)) and then deriving the diagnostic variables from this dataset.

In the objective analysis it was found that the value of the 'vertical radius of influence' required by the analysis procedure had quite a large impact on the resulting fields, essentially because it determined the vertical extent across which the surface observations exerted an influence. After experimentation this radius was set to 1km. This gave the most realistic-looking vertical structure in patterns of potential temperature and wet-bulb potential temperature. Other radii gave, in the lowest 100 to 200hPa, either large superadiabatic lapse rates or large stratification (which over a warm sea could not be maintained). The suggestion that there *should* be little variation in theta-W in the lowest 100-200hPa of a very unstable airmass with a long sea track was investigated by inspecting Thorshavn, Lerwick and Stornoway soundings pertaining to the polar low outbreak. The range of theta-W values apparent below 800hPa on each was noted, and the mean of these ranges calculated. It was just 0.8°C.

References:

Aakjaer, P.D. 1992. Polar lows affecting Denmark. *Tellus,* **44A**, 155-172.

Batten, L.J. 1973. Radar observations of the atmosphere. University of Chicago Press, Chicago.

Bell, R.S. 1994. The assimilation of ERS-1 scatterometer winds. Forecasting Research Division Technical Report no. 89. Meteorological Office, Bracknell. 41 pages.

Bennetts, D.A. and Hoskins, B.J. 1979. Conditional symmetric instability - a possible explanation for frontal rainbands. *Quart J. R. Met. Soc.*, **105**, 945-962.

Browning, K.A. and Hill, F.F. 1985. Mesoscale analysis of a polar trough interacting with a polar front. *Quart J. R. Met. Soc.*, **111**, 445-462.

Browning, K.A. and Roberts, N. 1994. Structure of a frontal cyclone. *Quart. J. R. Met. Soc.*, **120**, 1535-1557.

Businger, S. 1985. The synoptic climatology of polar low outbreaks. *Tellus*, **37A**, 419-432.

Carleton, A.M., McMurdie, L.A., Zhao, H., Katsaros, K.B., Mognard, N.M. and Claud C., March 1993. Satellite microwave sensing of Antarctic Ocean mesocyclones, Proceeding of the 4th AMS South. Hemisph. Met. Conf., New Zealand, 497-498.

Chedin, A., and Scott, N.A., 1985. Initialization of the radiative transfer equation inversion problem from a pattern recognition type approach. Applications to the satellites of the TIROS-N series, Advances in Remote Sensing Retrievals, Academic Press, A. Deepak Ed., 495-515.

Chedin, A., Scott N.A., Wahiche, C. and Moulinier, P., 1985. The Improved Initialisation Inversion Method : a high resolution physical method for temperature retrievals from satellites of the TIROS-N series, *J. Clim. Appl. Meteorol.*, **24**, 124-143.

Claud, C., Scott, N.A. and Chedin, A., 1992. Use of TOVS observations for the study of polar and arctic lows, *Int. J. of Remote Sens.*, **13 (1)**, 129-139.

Claud, C., Mognard, N.M., Katsaros, K.B., Chedin, A. and Scott, N. A., 1993. Satellite observations of a polar low over the Norwegian Sea by Special Sensor Microwave Imager, Geosat, and TIROS-N Operational Vertical Sounder, *J. Geophys. Res.*, **98** (C8), 14487-14506.

Clough, S.A. and Franks, R.A.A. 1991. The evaporation of frontal and other stratiform precipitation. *Q. J. R. Met. Soc.*, **117**. 1057-1080.

Cullen, M.J.P. 1991. The Unified Forecast/Climate Model. Short-Range Forecasting Research Division Scientific Paper No. 1.

Duncan, C.N., 1978. Baroclinic instability in a reversed shear flow. *Meteorol. Mag.* **107**, 17-23.

Emmanuel, K.A. 1983a. The Lagrangian parcel dynamics of moist symmetric instability. *J. Atmos. Sci.*, **40**, 2368-2376.

Emmanuel, K.A. 1983b. On assessing local conditional symmetric instability from atmospheric soundings. *Mon. Wea. Rev.*, **111**, 2016-2033.

Escobar, J., Base de donnees pour la restitution de parametres atmospheriques a l'echelle globale; Etude sur l'inversion par reseaux de neurones des donnees des sondeurs verticaux atmospheriques satellitaires presents et a venir, 1993. PhD dissertation (in French), Universite Pierre et Marie Curie. Available from Laboratoire de Meteorologie Dynamique, Ecole Polytechnique, 91128 Palaiseau Cedex, France.

Forbes, G.S. and Lottes, W.D. 1985. Classification of mesoscale vortices in polar airstreams and the influence of the large-scale environment on their evolutions. *Tellus*, **37A**, 132-155.

Gronas, S. and Kvamsto, N.G. (1994) Synoptic conditions for arctic front polar lows. in 'The Life Cycles of Extratropical Cyclones' III, 89-95. Proceedings of an international symposium. Almer Mater Forlag AS, Bergen.

Gyakum, J.R. (1983) On the Evolution of the *QEII* Storm. I: Synoptic Aspects. *Mon Wea Rev*, **111**, 1137-1155.

Gyakum, J.R., Roebber, P.J. and Bullock, T.A. (1992) The role of antecedent vorticity development as a conditioning process in explosive cyclone intensification. *Mon Wea Rev*, **120**, 1465-1489.

Harrold, T.W. and Browning, K.A. 1969. The polar low as a baroclinic disturbance. *Quart. J. R. Met. Soc.* **95**, 710-723.

Hewson, T.D. 1993a. Orographic cirrus generated by Iceland and the Faeroe islands - 4th-6th May, 1993. *Meteorol Mag*, **122**. 249-253.

Hewson, T.D. 1993b. The Fronts 92 Experiment: A Quicklook Atlas. JCMM internal report no. 15. Meteorological Office. Bracknell. 176 pages.

Locatelli, J.D., Hobbs, P.V. and Werth, J.A. 1982. Mesoscale structures of vortices in polar airstreams. *Mon Wea Rev.*, **110**, 1417-1433.

Locatelli, J.D., Martin, J.E. and Hobbs, P.V. 1994. A wide cold-frontal rainband and its relationship to frontal topography. *Q. J. R. Met. Soc.* **120**, 259-275.

Ludlam, F.H. 1980. Clouds and storms: the behaviour and effect of water in the atmosphere. The Pennsylvania State University Press. 405 pages.

Lyall, I.T. 1972. The polar low over Britain. *Weather*, **27**, 378-390.

Mansfield, D.A. 1974. Polar lows: the development of baroclinic disturbances in cold air outbreaks. *Q. J. R. Met. Soc.* **100**. 541-554.

Matrosov, S.Y. 1992. Radar Reflectivity in Snowfall. *IEEE Transactions on Geoscience and Remote Sensing*, **30**, 454-461.

Mcginnigle, J.B. 1990. Numerical weather prediction model performance on instant occlusion developments. *Meteorol Mag*, **119**, 149-163.

Meteorological Office. 1987. The storm of 15/16 October 1987. Meteorological Office, Bracknell.

Meteorological Office. 1993. Forecaster's Reference Book. Meteorological Office, Bracknell.

Neiman, P.J. and Shapiro, M.A (1993) The Life Cycle of an Extratropical Marine Cyclone. Part I: Frontal-Cyclone Evolution and Thermodynamic Air-Sea Interaction. *Mon Wea Rev.* **121**, 2153-2176.

Neiman, P.J., Shapiro, M.A and Fedor, L.S. (1993) The Life Cycle of an Extratropical Marine Cyclone. Part II: Mesoscale Structure and Diagnostics. *Mon Wea Rev.* **121**, 2177-2199.

Norris, J. and Young, M.V. (1991) Satellite photograph - 2 February 1991 at 1533 UTC. *Meteorol Mag, 120, 115-116*

Parker, D.J. and Thorpe, A.J. 1994. Convective Frontogenesis. JCMM internal report no. 27. Meteorological Office, Bracknell. 44 pages.

Pedder, M. A. (1993) Interpolation and filtering of spatial observations using successive corrections and Gaussian filters, *Mon. Wea. Rev.*, **121**, 2889-2902.

Pike, W.S. 1990a. Radar study of the snowfall in south-west Cornwall on 12 January 1987. *Meteorol Mag*, **119**, 97-102.

Pike, W.S. 1990b. A heavy mesoscale snowfall event in northern Germany, *Meteorol Mag*, **119**, 187-195.

Rasmussen, E. 1985. A case study of a polar low development over the Barents Sea, *Tellus*, **37A**, 407-418.

Rasmussen, E.A. and Aakjaer, P.D. 1992. Two polar lows affecting Denmark, *Weather*, **47**, 326-338.

Reed, R.J. and Duncan, C.N. 1987. Baroclinic Instability as a mechanism for the serial development of polar lows: a case study. *Tellus*, **39A**, 376-384.

Shapiro, M.A., Fedor, L.S. and Hampel, T., 1987. Research aircraft measurements of a polar low over the Norwegian Sea. *Tellus*, **39A**, 272-306.

Shapiro, M.A. and Keyser, D., 1990: Fronts, jet streams and the tropopause. *Extratropical Cyclones, The Erik Palmen Memorial Volume*, C.W. Newton and E. Holopainen, Eds., Amer. Meteor. Soc., 167-191.

Shutts, G.J. (1990) Dynamical aspects of the October storm 1987: A study of a successful fine-mesh simulation. *Q J R Meteorol Soc*, **116**, 1315-1347.

Smith, W.L., Woolf, H.M., Hayden, C.M., Wark, D.Q. and McMillin, L.M. 1979. The TIROS-N Operational Vertical Sounder, *Bull. Am. Meteorol. Soc.*, **60**(10), 1177-1187.

Turner, J., Lachlan-Cope, T.A., Warren, D.E. and Duncan, C.N. 1993 A mesoscale vortex over Halley Station, Antarctica, *Mon. Wea. Rev.*, **121**(5), 1317-1336.

Young, M.V. 1990. Satellite and radar images, 0900GMT on 3 February 1990. *Weather*. **45**. 268-270.

CURRENT JCMM INTERNAL REPORTS

This series of JCMM Internal Reports, initiated in 1993, contains unpublished reports and also versions of articles submitted for publication. The complete set of Internal Reports is available from the National Meteorological Library on loan, if required.

1. **Research strategy and programme**
   K A Browning et al
   January 1993

2. **The GEWEX Cloud System Study (GCSS)**
   GEWEX Cloud System Science Team
   January 1993

3. **Evolution of a mesoscale upper tropospheric vorticity maximum and comma cloud from a cloud-free two dimensional potential vorticity anomaly**
   K A Browning
   January 1993

4. **The global energy and water cycle**
   K A Browning
   July 1993

5. **Structure of a midlatitude cyclone before occlusion**
   K A Browning and N Roberts
   July 1993

6. **Developments in systems and tools for weather forecasting**
   K A Browning and G Szejwach
   July 1993

7. **Diagnostic study of a narrow cold frontal rainband and severe winds associated with a stratospheric intrusion**
   K A Browning and R Reynolds
   August 1993

8. **Survey of perceived priority issues in the parametrizations of cloud-related processes in GCMs**
   K A Browning
   September 1993

9. **The effect of rain on longwave radiation**
   I Dharssi
   September 1993

10. **Cloud microphysical processes - a description of the parametrization used in the large eddy model**
    H Swann
    October 1993

11. **An appreciation of the meteorological research of Ernst Kleinschmidt**
A J Thorpe
May 1992

12. **Potential vorticity of flow along the Alps**
A J Thorpe, H Volkert and Dietrich Heimann
August 1992

13. **The representation of fronts**
A J Thorpe
January 1993

14. **A parametrization scheme for symmetric instability: test for an idealised flow**
C S Chan and A J Thorpe
February 1993

15. **The Fronts 92 Experiment: a Quicklook Atlas**
Edited by T D Hewson
November 1993

16. **Frontal wave stability during moist deformation frontogenesis**
Part 1: Linear wave dynamics
C H Bishop and A J Thorpe
May 1993

17. **Frontal wave stability during moist deformation frontogenesis**
Part 2. The suppression of non-linear wave development
C H Bishop and A J Thorpe
May 1993

18. **Gravity waves in sheared ducts**
S Monserrat and A J Thorpe
October 1993

19. **Potential vorticity and the electrostatics analogy: quasi-geostrophic theory**
C Bishop and A J Thorpe
November 1993

20. **Recent advances in the measurement of precipitation by radar**
A J Illingworth
April 1993

21. **Micro-physique et givrage: cloud microphysics and aircraft icing**
A J Illingworth
May 1993

22. **Differential phase measurements of precipitation**
M Blackman and A J Illingworth
May 1993

23. **Estimation of effective radius of cloud particles from the radar reflectivity**
N I Fox and A J Illingworth
May 1993

24. **A simple method of Dopplerising a pulsed magnetron radar**
A Hua, A J Illingworth and J Eastment
November 1993

25. **Radiation and polar lows**
George C Craig
February 1994

26. **Collected preprints submitted to the International Symposium on the Life Cycles of Extratropical Cyclones; Bergen, Norway, 27 June - 1 July 1994**
April 1994

27. **Convective frontogenesis**
Douglas J Parker and Alan J Thorpe
April 1994

28. **Improved measurement of the ice water content in cirrus using a total water evaporator**
Philip R A Brown and Peter N Francis
April 1994

29. **Mesoscale effects of a dry intrusion within a vigorous cyclone**
K A Browning and B W Golding
April 1994

30. **GEWEX Cloud System Study, Science Plan**
May 1994

31. **Parametrization of momentum transport by convectively generated gravity waves**
R Kershaw
May 1994

32. **Mesoscale Modelling Newsletter No 5**
May 1994

33. **Observations of the mesoscale sub-structure in the cold air of a developing frontal cyclone**
K A Browning, S A Clough, C S A Davitt, N M Roberts and T D Hewson
May 1994

34. **Longwave radiative forcing of a simulated tropical squall line**
Imtiaz Dharssi
July 1994

35. **On the nature of the convective circulation at a kata-cold front**
K A Browning
September 1994

36. **Collective preprints of papers submitted to the COST-75 International Seminar on Advanced Weather Radar Systems, Brussels, 20-23 September 1994**
November 1994

37. **Use of satellite imagery to diagnose events leading to frontal thunderstorms: Parts I and II of a case study**
K A Browning and N M Roberts
November 1994

38. **The role of spaceborne millimetre-wave radar in the global monitoring of ice cloud**
P R A Brown, A J Illingworth, A J Heymsfield, G M McFarquhar, K A Browning and M Gosset
December 1994

39. **Potential vorticity inversion**
Michal Ziemianski
October 1994

40. **Theory of mature tropical cyclones; a comparison between Kleinschmidt (1951) and Emanuel (1986)**
Suzanne L Gray
December 1994

41. **Dispersion and removal of pollutants during the passage of an atmospheric frontal system**
N R Gimson
December 1994

42. **The role of snow sublimation in frontogenesis**
D J Parker and A J Thorpe
December 1994

43. **Potential vorticity and the electrostatics Analogy: Ertel-Rossby formulation**
A J Thorpe and C H Bishop
December 1994

44. **Mesoscale aspect of extratropical cyclones: an observational perspective**
K A Browning
January 1995

45. **A polar low outbreak: evolution and mesoscale structures**
T D Hewson, G C Craig and C Claud
February 1995

Met Office Joint Centre for Mesoscale Meteorology Department of Meteorology
University of Reading PO Box 243 Reading RG6 6BB United Kingdom
Tel: +44 (0)118 931 8425 Fax: +44 (0)118 931 8791
www.metoffice.com